

Atmospheric correction for satellite-based volcanic ash mapping and retrievals using “split window” IR data from GOES and AVHRR

Tianxu Yu and William I. Rose

Department of Geological Engineering and Sciences, Michigan Technological University, Houghton, Michigan, USA

A. J. Prata

CSIRO, Division of Atmospheric Research, Aspendale, Victoria, Australia

Received 2 April 2001; revised 29 August 2001; accepted 17 September 2001; published 29 August 2002.

[1] Volcanic ash in volcanic clouds can be mapped in two dimensions using two-band thermal infrared data available from meteorological satellites. *Wen and Rose* [1994] developed an algorithm that allows retrieval of the effective particle size, the optical depth of the volcanic cloud, and the mass of fine ash in the cloud. Both the mapping and the retrieval scheme are less accurate in the humid tropical atmosphere. In this study we devised and tested a scheme for atmospheric correction of volcanic ash mapping and retrievals. The scheme utilizes infrared (IR) brightness temperature (BT) information in two infrared channels (both between 10 and 12.5 μm) and the brightness temperature differences (BTD) to estimate the amount of BTD shift caused by lower tropospheric water vapor. It is supported by the moderate resolution transmission (MODTRAN) analysis. The discrimination of volcanic clouds in the new scheme also uses both BT and BTD data but corrects for the effects of the water vapor. The new scheme is demonstrated and compared with the old scheme using two well-documented examples: (1) the 18 August 1992 volcanic cloud of Crater Peak, Mount Spurr, Alaska, and (2) the 26 December 1997 volcanic cloud from Soufriere Hills, Montserrat. The Spurr example represents a relatively “dry” subarctic atmospheric condition. The new scheme sees a volcanic cloud that is about 50% larger than the old. The mean optical depth and effective radii of cloud particles are lower by 22% and 9%, and the fine ash mass in the cloud is 14% higher. The Montserrat cloud is much smaller than Spurr and is more sensitive to atmospheric moisture. It also was located in a moist tropical atmosphere. For the Montserrat example the new scheme shows larger differences, with the area of the volcanic cloud being about 5.5 times larger, the optical depth and effective radii of particles lower by 56% and 28%, and the total fine particle mass in the cloud increased by 53%. The new scheme can be automated and can contribute to more accurate remote volcanic ash detection. More tests are needed to find the best way to estimate the water vapor effects in real time. *INDEX TERMS*: 0370 Atmospheric Composition and Structure: Volcanic effects (8409); 8419 Volcanology: Eruption monitoring (7280); 0305 Atmospheric Composition and Structure: Aerosols and particles (0345, 4801); *KEYWORD*: volcanic clouds

1. Introduction

[2] Infrared data using two bands in the 10–12 μm region has been used successfully to detect atmospheric particles because the transmittances of many particles display strong spectral variation in this spectral region, and the atmosphere over this region is fairly transparent. *Prata* [1989b] used a radiative transfer model to simulate the difference in temperature obtained at wavelengths of 10.8 μm and 11.9 μm when the volcanic cloud is viewed from space. His calculations indicated that the difference is due primarily to the much stronger dispersive nature of

silicate materials compared to water and ice particles in most meteorological clouds and that two-band infrared data can be used to detect and discriminate volcanic clouds from meteorological clouds. *Wen and Rose* [1994] presented a method to retrieve the size, optical depth, and total mass of silicate particles in volcanic clouds using two advanced very high resolution radiometer (AVHRR) thermal infrared bands (bands 4 and 5, Table 1). Band 4 minus band 5 brightness temperature difference (BTD) images are used in this model to discriminate volcanic clouds from the meteorological ones, because meteorological clouds generally have positive BTD [*Yamanouchi et al.*, 1987], whereas volcanic clouds have negative BTD [*Prata*, 1989a, 1989b; *Wen and Rose*, 1994; *Schneider et al.*, 1995]. Meteorological cloud pixels

Table 1. GOES and AVHRR Information

| Band | GOES 8 | | AVHRR | |
|------|------------------------------|-------------------|------------------------------|-------------------|
| | Wavelength, μm | Resolution, km | Wavelength, μm | Resolution, km |
| 1 | 0.55–0.75 | 1 | 0.58–0.68 | 1.1 |
| 2 | 3.8–4.0 | 4 | 0.725–1.10 | 1.1 |
| 3 | 6.5–7.0 | 8 | 3.55–3.93 | 1.1 |
| 4 | 10.2–11.2 | 4 | 10.3–11.3 | 1.1 |
| 5 | 11.5–12.5 | 4 | 11.5–12.5 | 1.1 |

typically form an arch-like array, while volcanic cloud pixels occur in an inverted arch-like field on a plot of band 4-band 5 (BTD) versus band 4 [Parol *et al.*, 1991].

[3] As the water vapor content of the lower troposphere increases, the absolute BTD values increase [Rose *et al.*, 1997]. Coll and Casselles [1997] showed that atmospheric water vapor differentially affects AVHRR and GOES (Geostationary Operational Environmental Satellite) infrared brightness temperatures. Simulations of the differential effects on AVHRR bands 4 and 5 by V. J. Realmuto (personal communication, 1998) have shown that the difference in bands 4 and 5 brightness temperatures can be several degrees. We are motivated in this work by the expectation that AVHRR and GOES data can be used to discriminate the volcanic clouds from meteorological clouds even over tropical ocean regions where the atmospheric water vapor content is high and where volcanic cloud pixels have positive BTD values.

[4] Detection and mapping of volcanic clouds is easy when the eruption is large and the optical depths of volcanic clouds are greater than 0.5. Eruptions such as El Chichón, which occurred in the tropics, produced large and clear volcanic cloud signals [Schneider *et al.*, 1999], but with weak eruptions, the problems increase. The existing discrimination scheme [Prata, 1989a; Wen and Rose, 1994; Schneider *et al.*, 1995] can map small volcanic clouds at high latitudes, but in moist tropical conditions, only the denser cores of the volcanic clouds can be mapped [Mayberry *et al.*, 2002], where the BTD is large enough to counteract the effects of atmospheric moisture.

[5] In this paper we investigate an atmospheric correction using standard atmospheric profiles and moderate resolution transmission (AVHRR) simulations of the effects of higher atmospheric water vapor content on GOES and AVHRR bands 4 and 5 data. We demonstrate the use of the modified discrimination scheme and the revised retrieval algorithm on GOES data from the Montserrat 26 December 1997 eruption and AVHRR data from the Spurr 18 August 1992 eruption. These two clouds are chosen because they represent two typical volcanic cloud atmospheric environments: one in a tropical region, the other from a subarctic region. Also, both were measured by an independent detector (Total Ozone Mapping Spectrometer) at nearly the same time.

[6] First we consider the areas of volcanic clouds detected by GOES and AVHRR thermal channels 4 and 5, comparing areas detected with and without atmospheric correction. This is meant to demonstrate the magnitude of the need for correction in the two test environments. The second part of the paper is the modification of the retrievals of volcanic properties such as optical depth, particle radius, and total mass. It also compares results with and without

atmospheric corrections. The third part of the paper is an evaluation of the environmental stability and practicality of the atmospheric corrections. It focuses on how the atmospheric corrections can be used in real-time retrievals of volcanic clouds.

2. Eruptions and Satellite Data

[7] On the morning of 26 December 1997 the dome at Soufriere Hills Volcano, Montserrat, collapsed and produced a pyroclastic density current, which convected and formed a column that rose several kilometers into the atmosphere [Cole *et al.*, 1998; Baxter *et al.*, 1999]. The volcanic ash cloud from this event was mapped and described by Mayberry *et al.* [2002] using GOES data. Her research is based on 33 GOES images of volcanic cloud collected over a period of about 17 hours (approximately every 30 min from 0709 to 2339 UT). She indicated that the volcanic cloud elongated hundreds of kilometers to the SE and simultaneously migrated 120 km to the SW throughout the ~ 17 hours. In the early parts of this eruption a volcanogenic meteorological cloud was generated from evaporation of seawater caused by the density current [Mayberry *et al.*, 2002]. By 1539 UT the volcanogenic meteorological cloud had dissipated, making the study of atmospheric effects on volcanic cloud retrievals more straightforward.

[8] GOES operates at the geosynchronous altitude of 35,800 km above the Earth's surface and has five spectral channels (Table 1). The scan mirror of the GOES need only scan 10° from the subsatellite point to view the entire hemisphere [Kidder and Vonder Haar, 1995]. Geostationary data are advantageous for studying volcanic clouds because of their fine temporal resolution. GOES provided 33 images of volcanic clouds from the Montserrat 26 December 1997 eruption. The old and new schemes for discrimination of volcanic clouds from meteorological ones were performed on six of the 33 images, and the retrieval of particle size, optical depth, and mass was done on the 1539 UT image. This image was chosen for a detailed study because it avoids the complexity of the volcanogenic meteorological cloud that occurred in earlier images and because it is very close to TOMS AI (aerosol index) data collection, which can be used as a validation of volcanic ash detection [Krotkov *et al.*, 1999].

[9] The Crater Peak eruption of Mount Spurr on 18 August 1992 produced about an order of magnitude more ash than the Montserrat eruption [Rose and Mayberry, 2000], and its volcanic cloud reached altitudes of more than 15 km [Rose *et al.*, 1995]. Six AVHRR images were collected during the first day of volcanic cloud drift [Schneider *et al.*, 1995]. In this research we focus on the 1857 UT image. Both the old and the new retrieval models are tested on this volcanic cloud, which was also used for TOMS AI volcanic ash validation study by Krotkov *et al.* [1999]. AVHRR is a broad band, four- or five-channel (depending on the model) scanner, sensing in the visible, near-infrared, and thermal infrared portions of the electromagnetic spectrum. The AVHRR sensor provides for global (pole to pole) onboard collection of data from all spectral channels. The satellite orbits the Earth 14 times each day from 833 km above its surface. The scan mirror of the

Table 2. Statistics of Montserrat and Spurr Classifications

| | Montserrat | | | | Spurr | | | |
|----------------------|------------------|---------------|----------------|----------|------------------|----------------|----------------|----------|
| | Band 4 BT Range | BTD Range | Mean Band 4 BT | Mean BTD | Band 4 BT Range | BTD Range | Mean Band 4 BT | Mean BTD |
| Volcanic cloud | 268.56 292.07 | -1.23 3.07 | 285.69 | 0.73 | 234.80 272.08 | -14.14 0.96 | 259.99 | -4.89 |
| Clear-sky over ocean | 294.91 297.37 | 0.64 2.85 | 296.65 | 1.78 | 273.23 275.12 | -0.39 0.87 | 274.42 | 0.08 |
| Clear-sky over land | 302.74 308.81 | 1.78 5.72 | 306.01 | 3.78 | 277.04 284.80 | 0.55 2.11 | 282.59 | 1.50 |
| Cloud over ocean | 226.66 296.67 | -2.39 5.55 | 288.60 | 1.67 | 219.94 273.99 | 0.02 2.79 | 260.94 | 0.94 |
| Cloud over land | 236.28 303.96 | -2.47 5.40 | 285.47 | 2.00 | 212.75 271.63 | -2.51 6.11 | 251.69 | 0.68 |

AVHRR scans 55.3° for the AVHRR to record 2048 samples centered on the subsatellite point [Kidder *et al.*, 1995]. The two thermal infrared bands of AVHRR are only slightly different from GOES (Table 1), and therefore very slightly altered retrieval schemes, which correct for the slight band shift, can be used for AVHRR and GOES.

3. Infrared Remote Detection of Volcanic Clouds

[10] To investigate whether an improved cutoff can be developed for volcanic cloud discrimination, we examined the classification of pixels in Montserrat and Spurr data in detail. Supervised classification (maximum likelihood) is a standard digital image-processing technique used in remote sensing [Jensen, 1996], where "pure" pixels in an image are used as training sets to develop an overall classification of all pixels. We applied this technique to the Montserrat and Spurr data using bands 4 and 5 of GOES and AVHRR. Training sets are selected on the basis of our image interpretation experience to represent different environmental conditions. Table 2 lists statistical information about the Montserrat and Spurr images. Image pixels are classified into five different groups: (1) volcanic clouds, (2) clear sky over ocean, (3) clear sky over land, (4) meteorological clouds over ocean, and (5) meteorological clouds over land. Figures 1a and 1b, respectively, show selected pixels from each group plotted on band 4 versus BTD for the 1539 UT image of Montserrat volcanic cloud and 1857 UT image of Spurr volcanic cloud.

[11] In the Montserrat and Spurr examples (Figures 1a and 1b), most meteorological cloud pixels have positive BTD values, reflecting the dominant effects of liquid water and ice particles which cause a positive BTD. Volcanic cloud pixels for both examples include many negative BTD values because of the effect of silicates. Some volcanic cloud pixels have positive BTD values, however. Volcanic cloud pixels with positive BTD values are incorrectly eliminated if a cutoff procedure $BTD < 0$ is used. It is not possible to correct this with a simple cutoff BTD shift in a positive direction. If a procedure such as $BTD < 2$ or $BTD < 3$ is used, large numbers of meteorological cloud and clear-sky pixels with positive BTD are incorrectly included with volcanic cloud pixels. An improved volcanic cloud discrimination procedure therefore must include the volcanic cloud pixels with a positive BTD while eliminating other pixels that also have a positive BTD.

[12] At Montserrat (Figure 1a), clear sky over land pixels and clear sky over ocean pixels have a higher BT (>292 K) and a $BTD > 0$; meteorological cloud over land pixels and meteorological cloud over ocean pixels have a wide BT range (usually a $BTD > 0$), while volcanic cloud pixels mainly have a $BT < 292$ K. At Spurr (Figure 1b) the results are quite similar: clear sky over land pixels and clear sky over ocean pixels have a higher BT (>272 K) and a $BTD > 0$; meteorological cloud over land pixels and meteorological cloud over ocean pixels have a wide BT range (usually with a $BTD > 0$), while volcanic cloud pixels mainly have a $BT < 272$ K. Volcanic cloud pixels have a BT of 270–290 K and 260–s272 K, respectively, for Montserrat and Spurr (Figures 1a and 1b) and represent part of an inverted arch-like field on a plot of band 4 versus BTD (Figures 5 and 6) as we mentioned before.

[13] The cutoff to discriminate volcanic clouds without atmospheric correction uses BTD values alone and a cutoff such as $BTD < -0.2$ or $BTD < 0$, a straight line parallel to AE in Figure 1. In this paper we use a new cutoff procedure based on both BTD and BT values. Figure 1 illustrates the new procedure for discrimination of volcanic cloud pixels from meteorological ones. The position of points C and D in Figure 1 is defined by the clear-sky ocean BTD and BT. For Montserrat (Figure 1a) we use values (292; 3) for C and (292; 0) for D, while B is (274; 0). For Spurr (Figure 1b), C and D are (272; 1) and (272; -0.5), while B is (260; -0.5). Pixels located below the line ABCDE are considered to be volcanic cloud pixels if atmospheric conditions are considered, while the old scheme interprets only pixels below the line AE as volcanic cloud pixels. Results from the two discriminations are contrasted in Figures 2 and 3. The old cutoff is more conservative. It eliminates almost all other kinds of pixels and defines a smaller cloud map that shows only the dense cores of the whole cloud (Figures 2b and 3b). The new procedure includes volcanic cloud signals that are too weak to counteract the effects of water vapor and will include false signals (Figure 1a). Potential volcanic cloud areas (Figures 2c and 3c) detected by the new procedure are larger than those from the old procedure, but they include false signals in the surrounding area. To eliminate these false signals, we develop an image-processing "near-neighbor" procedure that will exclude pixels not connected to a cloud mass with a core that has $BTD < 0$. Results of this further image processing are shown in Figures 2d and 3d

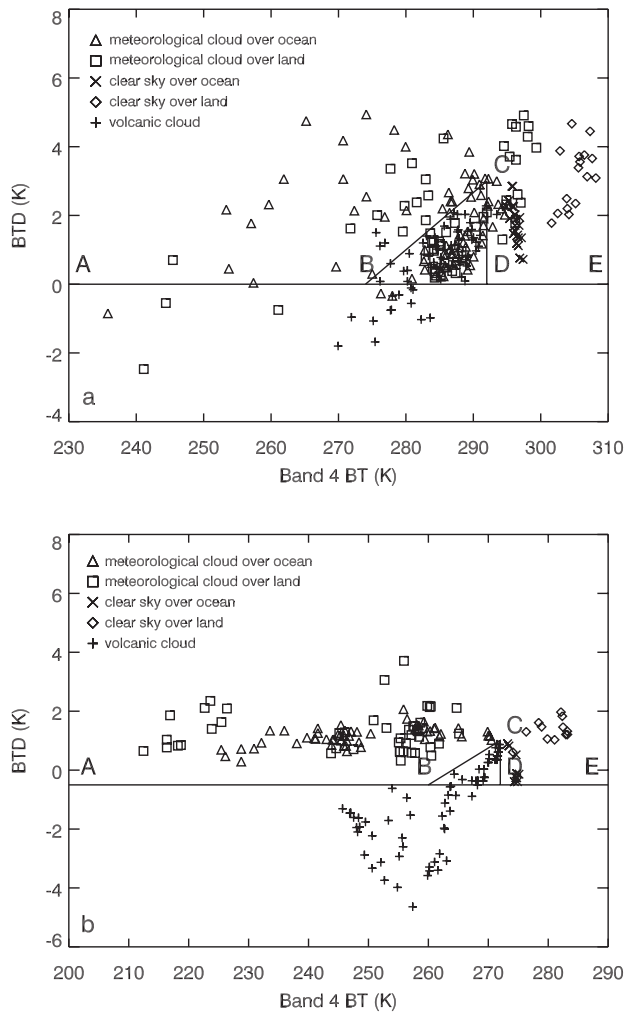


Figure 1. Graphical representation of old and new volcanic cloud cutoff procedure with representative pixel values plotted for each test case. (a) Band 4 versus BTD plot of different environmental conditions for Montserrat cloud. (b) Band 4 versus BTD plot of different environmental conditions for Spurr cloud. The old cutoff procedure only detects volcanic cloud pixels below the line AE, while for the atmospherically corrected new scheme, the pixels below the line ABCDE represent the volcanic cloud. Note that the size of the triangular wedge BCD is much larger for the moist tropical case of Montserrat.

for the Montserrat and Spurr volcanic clouds, respectively. The resulting refined images of volcanic clouds match very well the size of the clouds as observed with band 4 BT images (Figures 2a and 3a).

[14] Figure 4 shows how the Montserrat volcanic cloud area changed with time during the day 26 December 1997. Areas detected by the old and new procedures are illustrated. The volcanic cloud area increased in size rapidly at first, reached a maximum about 1600 UT, then decreased slowly in size. The areas discriminated by the new scheme were nearly 6 times larger than the areas detected by the traditional BTD cutoff procedure during much of the day. The large difference in area occurs mainly because the Montserrat volcanic eruption was small relative to other

eruptions [Mayberry *et al.*, 2002]; the concentration of fine ash in the clouds was not high enough to override the effects of the high humidity in the lower troposphere in the tropics. The old discrimination scheme cannot detect volcanic cloud pixels with positive BTD values which occur in the cloud edges. For the Montserrat volcanic cloud at 1539 UT, 26 December 1997, the new discrimination procedure detects a volcanic cloud area of $\sim 74,600 \text{ km}^2$, while the traditional procedure detects a volcanic cloud area of $\sim 13,200 \text{ km}^2$, a difference of a factor more than 5.

[15] The volcanic cloud areas detected by the old and new cutoff procedure for the 1857 UT Spurr cloud are $\sim 187,900$ and $\sim 283,700 \text{ km}^2$, respectively, an increase of $\sim 50\%$, much less than that for Montserrat. This smaller increase is probably explained by the dryer atmosphere of the subarctic. We also note that the area added represents generally very low optical depth and low ash concentrations.

[16] To verify the scale of the volcanic ash cloud, we used Nimbus 7 TOMS data for the Spurr cloud collected 4 min after the AVHRR and Earth Probe TOMS data collected at 1543 UT, 4 min after GOES, for the Montserrat cloud. The aerosol index (AI) can be derived from TOMS UV data to detect volcanic ash and other types of absorbing aerosols. AI is nearly zero for meteorological (water) clouds, and for absorbing aerosols, AI is positive and increases as the aerosol optical depth and aerosol layer height increase. AI also has the ability to detect UV-absorbing aerosols in the presence of subpixel clouds, thus ash clouds with water droplets and/or ice particles can be detected [Krotkov *et al.*, 1999]. Mayberry *et al.* [2002] compared the Montserrat volcanic cloud area detected by TOMS AI and band 4 BT; she showed that TOMS AI can outline the volcanic ash more fully than uncorrected GOES or AVHRR data. Area comparisons show clearly that for Montserrat the TOMS AI sees a cloud similar in size ($\sim 8 \times 10^4 \text{ km}^2$) to the cloud defined by the new scheme. For the Spurr cloud the TOMS AI sees a cloud that is nearly the same as the uncorrected scheme, while the atmospherically corrected cloud is about 50% larger. Since the additional Spurr volcanic cloud area detected by the new scheme is optically very thin, it may not be detected by TOMS AI, partly because TOMS has much lower spatial resolution. Taken together, these comparisons highlight the important use of TOM AI to judge atmospheric and environmental variables that affect the split window ash detection.

4. Retrieval Model

[17] The cutoff scheme described above is used to map the extent of the volcanic cloud in two dimensions, and it is also used to identify the pixels used in retrieval of particle size, optical depth, and mass of particles in the volcanic clouds [Wen and Rose, 1994]. The volcanic cloud in this model is assumed to be a single layer and parallel to the Earth's surface; the atmosphere above the volcanic cloud and between the surface and the cloud are assumed to be clear windows (effects of nonvolcanic aerosol particles are ignored); in this case the observed radiance I_{obsi} in a narrow band i centered at a wavelength λ_i is composed of radiation that is emitted from the cloud and the radiation emitted from the Earth's surface and then subsequently transmitted

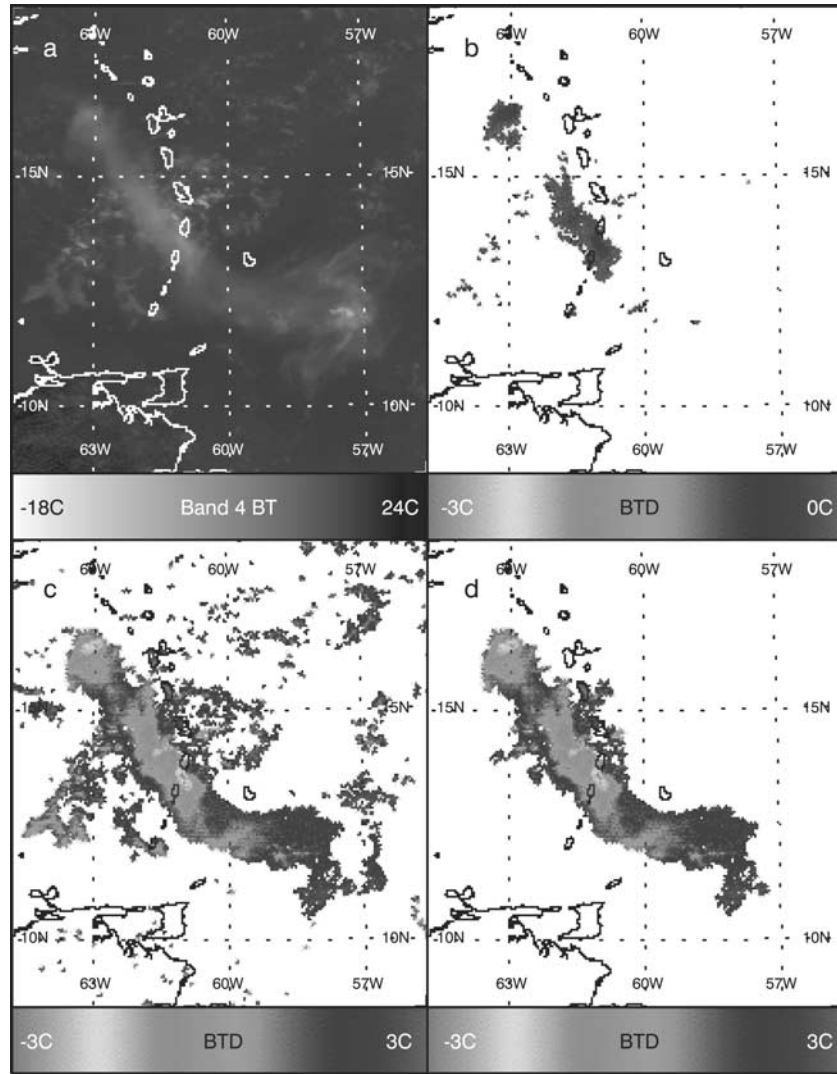


Figure 2. Comparison of new and old cutoff procedures for the Montserrat volcanic eruption. (a) Band 4 image of volcanic cloud area, where the volcanic cloud is depicted as grey over a black ocean background. (b) Volcanic cloud area using the old cutoff procedure. (c) Potential volcanic cloud area using the new cutoff procedure. (d) Final volcanic cloud area from the new cutoff procedure, with image processing to remove false signals (see text for explanation). See color version of this figure at back of this issue.

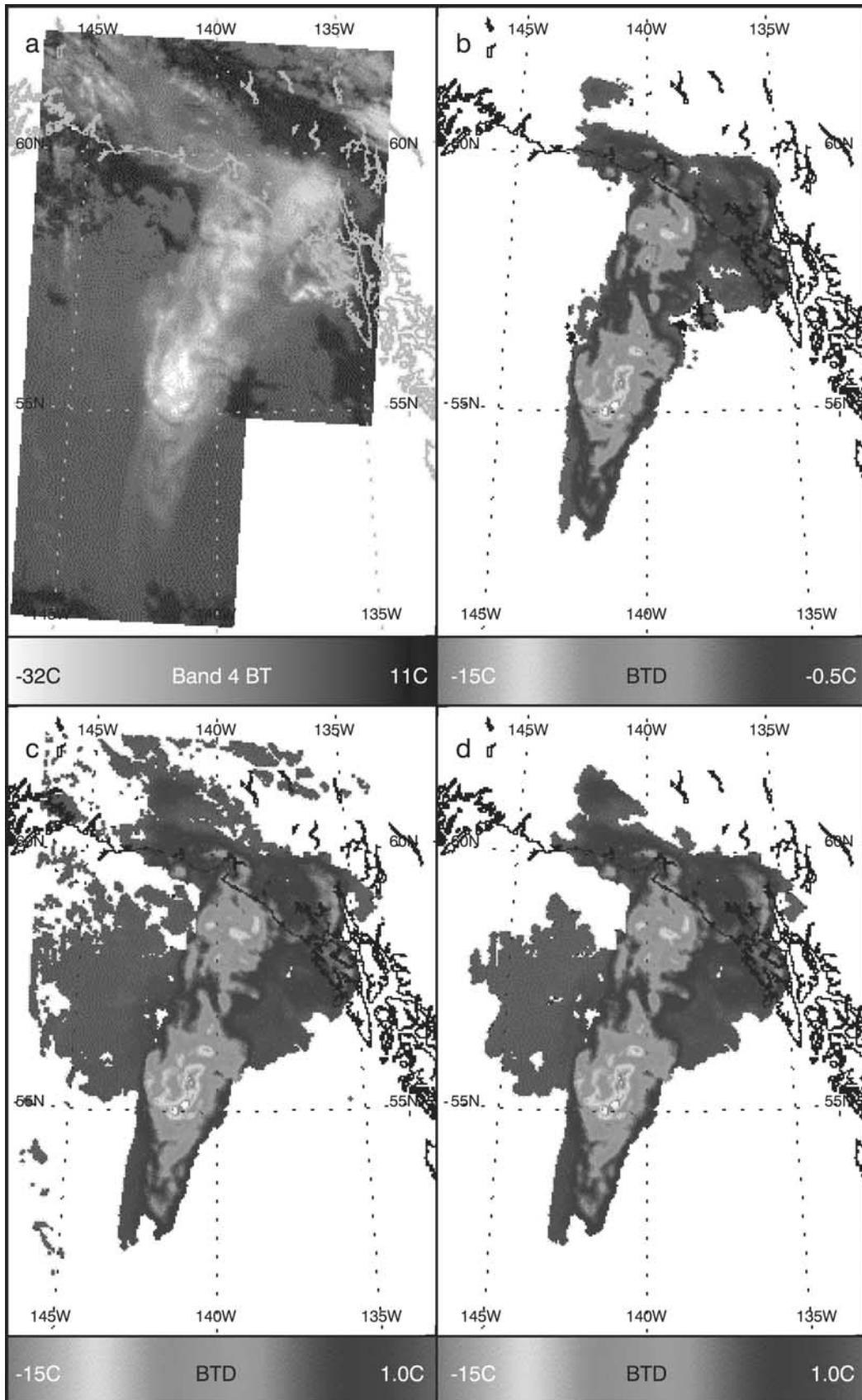
through the cloud; this observed radiance can be expressed by the following equations:

$$I_{\text{obs}4} = t_4 B(T_s) + e_4 B(T_c), \quad (1)$$

$$I_{\text{obs}5} = t_5 B(T_s) + e_5 B(T_c), \quad (2)$$

where I_{obs} is the radiance observed by the sensor at the cloud top by bands 4 and 5; t is the cloud transmittances of the two thermal bands, respectively; e is the cloud emissivity; T_s is the Earth surface temperature below the cloud; T_c is the cloud temperature and B is the Planck function. The first term on the right-hand side of the equation is the radiance that is transmitted through the cloud; the second term stands for the radiance emitted from the cloud top.

[18] The transmissivities t and emissivities e in equations (1) and (2) depend on cloud particle properties such as particle size, particle size distribution, optical depth, and the index of refraction of the particle. In our study the volcanic cloud is assumed to contain only andesite particles, and indices of refraction of andesite from *Pollack et al.* [1973] are used. The particle size distribution is assumed to be lognormal with a standard deviation of 0.74 [*Wen and Rose, 1994*], and the andesite particles are assumed to be spherical with a density of 2.6 g/cm^3 [*Neal et al., 1994*]. The emissivity e and transmissivity t can be expressed as functions of cloud optical depths (τ), the single-scattering albedo (ω), and the asymmetric parameter (g); that is, $e = f(\tau, \omega, g)$ and $t = f(\tau, \omega, g)$, where the single-scattering albedo ω , the asymmetric parameter g , and the optical depth τ are wavelength dependent. Mie theory is used, assuming that the particles are spherical. We compute the



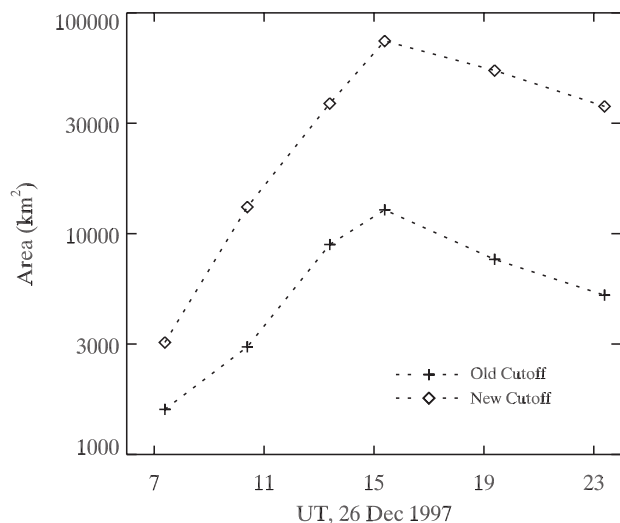


Figure 4. Volcanic cloud areas detected by new and old cutoff procedures for Montserrat volcanic cloud (see text for explanation).

single-scattering albedo ω and the asymmetric parameter g at the wavelength of the two thermal bands of AVHRR and GOES for a given effective radius. Eddington's approximation [Liou, 1980] is employed to compute the transmissivities t and emissivities e . The Eddington approximation is chosen because it solves the radiative transfer equations analytically and gives a fairly good accuracy for optically thick clouds. It should be used with care for optically thin cases when large absorption is involved. The *Wen and Rose* [1994] model is used to retrieve volcanic cloud properties for a given pair of cloud top temperature T_c and Earth surface temperature T_s by using a two-dimensional (2-D) look-up table with entries at prescribed values of mean particle size r and optical depth τ . Each pixel has a band 4 BT and BTM values. These are compared with the theoretically computed values within the look-up table, and the particle size r and optical depth τ , which make the best match, are assigned to that pixel. After obtaining the particle size r and optical depth τ for a pixel, the mass can be calculated for that pixel as detailed by *Wen and Rose* [1994], and the pixels can then be summed for a total fine ash mass in the cloud.

[19] Figures 5a and 6a, respectively, show the computed retrieval nets for Montserrat and Spurr volcanic clouds from *Wen and Rose* [1994]. The retrieval net is labeled for specific effective radius and optical depth values. Solid lines in Figures 5a and 6a represent different effective radii, and the dashed lines represent optical depth at $10.7 \mu\text{m}$. The solid lines and dashed lines converge at the left-hand and right-hand sides of the radius-optical depth envelopes. The converged point at the right-hand side is defined by the band 4 BT and BTM for the surface underneath the volcanic cloud; the converged point at the left-hand side is the

volcanic cloud temperature defined by the optically thick situation where no transmitted radiances from the Earth occur. Actual volcanic cloud pixels are superimposed as small dots on the theoretically calculated lines. The *Wen and Rose* [1994] model is based on equations (1) and (2), which assumes that there is no absorption of infrared radiation by atmospheric water vapor, so a single Earth surface temperature T_s can be used in equations (1) and (2); the BTM at converged points on the retrieval nets is zero. Figures 5a and 6a show that many volcanic cloud pixels are located outside the retrievable area and have positive BTM values. These volcanic cloud pixels with positive BTM are detected by the new cutoff. Retrievals cannot be performed on volcanic pixels with positive BTM because in the *Wen and Rose* [1994] model the BTM of the surface under the cloud is assumed to be zero, which is incorrect because of water vapor effects.

[20] To accurately retrieve results considering atmospheric moisture, the temperatures T_s of the two bands must not be assumed to be equal in equations (1) and (2). The ratio of volcanic cloud pixels with positive BTM to volcanic cloud pixels with negative BTM may be significant (Figure 5a). For a volcanic cloud in the middle and high latitudes, such as the Spurr volcanic cloud where water vapor contents of the troposphere are smaller, the effect of water vapor is less, the ratio of volcanic cloud pixels with positive BTM to volcanic cloud pixels with negative BTM is lower (Figure 6a). To accommodate atmospheric correction, equations (1) and (2) can be rewritten as

$$I_{\text{obs}4} = t_4 B(T_{s4}) + e_4 B(T_c), \quad (3)$$

$$I_{\text{obs}5} = t_5 B(T_{s5}) + e_5 B(T_c). \quad (4)$$

[21] T_{s4} and T_{s5} in equations (3) and (4) are brightness temperatures at the two different wavelengths at cloud base. Other terms in equations (3) and (4) are identical to these in equations (1) and (2). The value of T_s is affected by the emissivity and temperature of the surface as well as radiances contributed/absorbed by the atmosphere between the ground and the cloud base. One way to estimate T_s is to use clear-sky temperatures at bands 4 and 5 and compute the radiances T_s using the Planck function. The clear-sky temperatures at bands 4 and 5 may be measured in clear-sky areas adjacent to the volcanic clouds. This method is reasonable because the atmosphere above the volcanic cloud is generally thin, contains few aerosol particles, and does not markedly affect the radiation transfer. Another way to estimate T_s is to use mathematical statistical methods such as those provided by *McMillan and Dean* [1982]. We chose to use MODTRAN (moderate resolution transmission) [Berk et al., 1989] to estimate upward radiance at the cloud base.

[22] MODTRAN is an atmospheric model developed over the past 25 years at the U.S. Air Force Phillips Laboratory. It is the recognized standard for computing

Figure 3. (opposite) Results of new and old cutoff procedures for Spurr volcanic eruption. (a) Band 4 image of volcanic cloud. (b) Volcanic cloud area depicted from the old cutoff procedure. (c) Volcanic cloud from the new cutoff procedure. (d) Final volcanic cloud area using the new cutoff procedure, and image processing to remove false signals (see text for explanation). See color version of this figure at back of this issue.

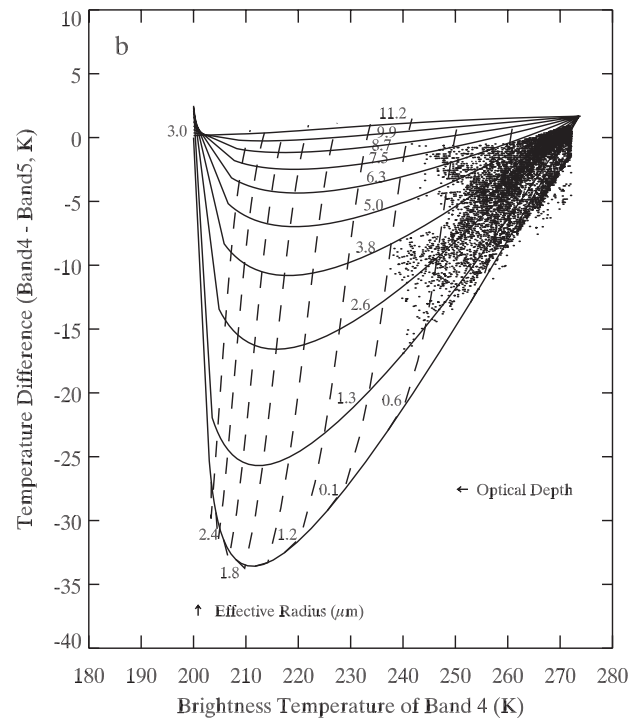
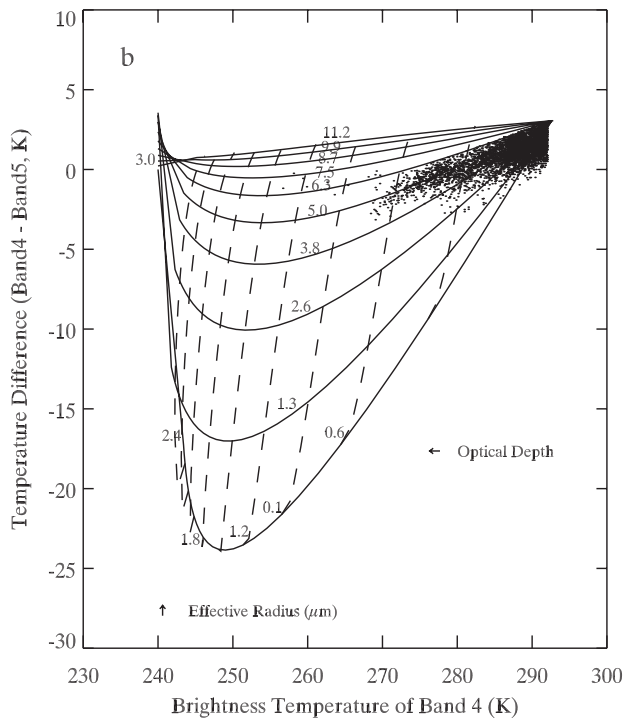
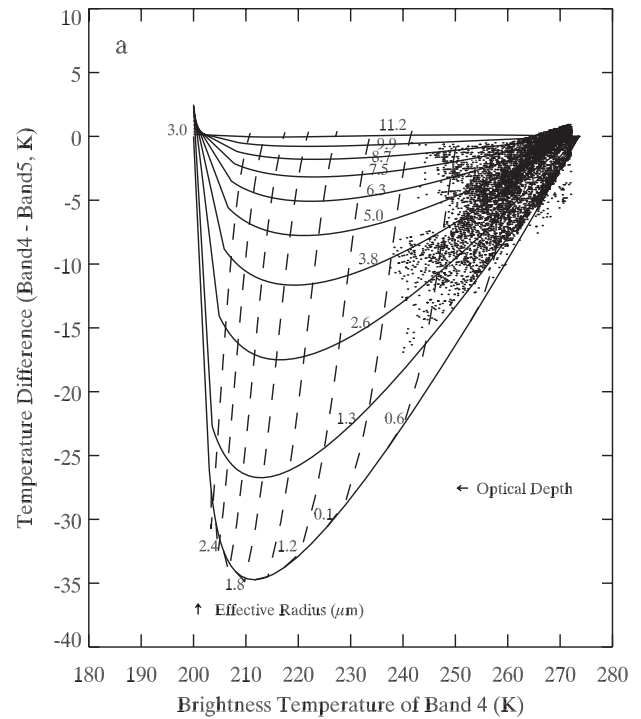
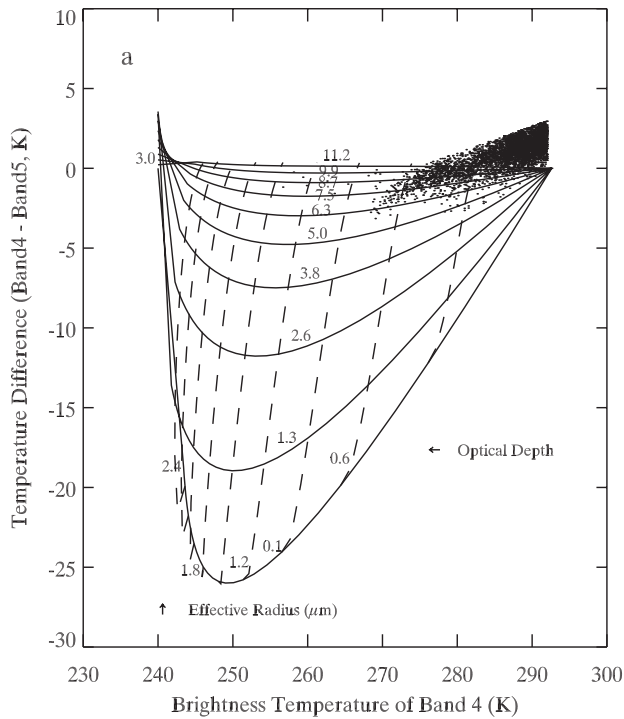


Figure 5. Retrieval grids of old and new retrieval models for Montserrat volcanic cloud. (a) The old retrieval model has many volcanic cloud pixels with positive BTD values located outside the retrievable area. Note triangular wedge of data which plots above the BTD = 0 line, as in Figure 1a. (b) New retrieval model with atmospheric corrections. Volcanic cloud pixels with positive BTD values are now mostly located inside the retrievable area. The ratio of volcanic pixels with positive BTD to volcanic pixels with negative BTD is large in this volcanic cloud example, which has a low optical depth and high atmospheric moisture.

Figure 6. Retrieval grids of old and new retrieval models for Spurr volcanic cloud. (a) Old retrieval model; many volcanic cloud pixels with positive BTD values are located outside the retrievable area. Note comparison with triangular wedge in Figure 1b. (b) New retrieval model with atmospheric corrections. Volcanic cloud pixels with positive BTD values are generally located inside the retrievable area. The ratio of volcanic pixels with positive BTD to volcanic pixels with negative BTD is small in this high-latitude example.

atmospheric transmissions and radiances at 2 cm^{-1} resolution. In our MODTRAN simulations, for simplicity and practicality, we use standard tropical and subarctic atmospheric profiles for the Montserrat and Spurr volcanic clouds, respectively. Thermal radiances with multiple scattering are considered, and no aerosol attenuation and cloud are included in the calculations. This assumption has the following advantages: (1) It corrects for the chronic gross differences in water vapor, which affect the tropics and high latitudes and (2) it avoids the need for a different procedure for each data set. The bands 4 and 5 brightness temperatures of the radiating surface under the volcanic cloud simulated from the MODTRAN are 292.62 and 289.57 K, respectively, for the Montserrat volcanic cloud. For the Spurr cloud the bands 4 and 5 brightness temperatures are 273.63 and 272.65 K, respectively. These two pairs of values match well the values we use in the discrimination procedure for Montserrat and Spurr volcanic clouds, which were measured in the images. The MODTRAN run results show that the subsurface temperature difference of bands 4 and 5 can reach a maximum of ~ 3.1 and ~ 1.0 K for the Montserrat and Spurr volcanic clouds. The main reason for the larger BT in the Montserrat cloud region is that the tropical atmosphere contains more water vapor than the subarctic atmosphere. MODTRAN simulations show that the water vapor density of the troposphere at tropical regions is about $639.4 \text{ g/cm}^2/\text{km}$, more than 3 times the water vapor density ($195.5 \text{ g/cm}^2/\text{km}$) at subarctic regions. We set the cloud top temperature to a value of 240 K for the 26 December 1999 Montserrat volcanic cloud based on measurements of the cloud when it was opaque [Mayberry *et al.*, 2002]. The cloud top temperature of the Spurr volcanic cloud is 200 K, which was also measured from the coldest part of the volcanic cloud earlier in the sequence of AVHRR images [Schneider *et al.*, 1995].

[23] Figures 5b and 6b show retrieval grids using the adjusted retrieval model for Montserrat and Spurr volcanic clouds; the main difference between Figures 5 and 6 is the shape of the right-hand top corner of the net which is controlled by the temperature of the Earth's surface underneath the volcanic cloud. Figures 5b and 6b thus reflect the positive BT phenomena of volcanic cloud. Most pixels with positive BT values now are within the grid in the retrievable area when the adjusted model is used, although a few pixels are still outside.

5. Real-Time Use of the Modified Retrieval Model

[24] Although MODTRAN is used in this paper to simulate the clear-sky brightness and BT under different atmospheric conditions, we are unsure if default atmospheric profiles in MODTRAN are adequate to represent the range of variation in real atmospheric profiles. For the Montserrat and Spurr volcanic clouds the subsurface is dominated by oceans. The climatological conditions in tropical regions, such as Montserrat during most of the year, are relatively stable (e.g., do not change much from day to day), while climatological conditions in the North Pacific region do change significantly and also show strong seasonality. The water vapor content of the atmosphere in the tropics is much higher than high-latitude regions and the effects on radiances transferred are much more profound,

but they are also more nearly constant, particularly for maritime locations.

[25] To investigate the patterns of spatial variation of BT and atmospheric moisture, we did MODTRAN simulations of the National Centers of Environmental Prediction (NCEP) analyses to depict the global distribution of BT and moisture on specific days. Detailed radiative transfer calculations were performed using the MODTRAN code to determine the top-of-the-atmosphere (TOA) brightness temperatures for the AVHRR 2 split-window channels. The calculations utilized global NCEP analyses for four different days and two different times. The days and times were chosen to represent seasonal and diurnal variations in atmospheric water vapor conditions. Figure 7 shows the TOA brightness temperature at $11 \mu\text{m}$ (bottom panel), the precipitable water amount (in centimeters), and the temperature difference ($T_4 - T_5$) between the $11 \mu\text{m}$ and the $12 \mu\text{m}$ AVHRR split window channels. The calculations shown are for 26 December 1996 at 0000 UT. The most notable feature of these calculations is the high degree of spatial correlation between the fields of precipitable water and $T_4 - T_5$. There is a marked nonlinear relationship between the TOA brightness temperature and the precipitable water. Similar results were found for the other days and times. Water vapor amount is not distributed uniformly over the globe. Largest amounts are found in tropical and subtropical regions, while the polar regions are relatively dry. Water vapor distributions also appear to follow weather systems, and the patterns resemble the cloud patterns associated with frontal systems. There also appears to be a strong correlation between warm ocean current systems and high water vapor loadings. These general patterns in water vapor amount (or precipitable water) are reflected in the global patterns of AVHRR BT.

[26] A semiempirical water vapor correction by Prata and Grant [2001b] suggested that there is a very strong correlation between precipitable water and BT and a strong but nonlinear correlation between precipitable water and top-of-the-atmosphere temperature at $11 \mu\text{m}$ or $12 \mu\text{m}$. This latter nonlinear relation derives from the correlation between the sea surface temperature (SST) and the precipitable water. Therefore there exists a nonlinear correlation between BT and T_4 through precipitable water. This fact is no surprise because it is the basis for estimating SST from the AVHRR and other instruments relying on the split window channels. Figure 8 shows the correlations between precipitable water (in centimeters) and $T_4 - T_5$, and T_4 and $T_4 - T_5$ calculated using RT and the NCEP data described earlier. The data shown are for 26 December 1996 at 0000 UT, but very similar results are obtained for other dates and times. Also shown in Figure 8 are empirical fits providing upper and lower bounds to the distribution of the points. The semiempirical relations describing these bounds are upper bound,

$$\Delta T_{\text{wv}} = \exp[20T^* - 18], \quad (5)$$

and lower bound,

$$\Delta T_{\text{wv}} = \exp[6T^* - b], \quad (6)$$

where $T^* = T_4/T_{\text{max}}$, and T_{max} is an arbitrary normalization constant assigned a value of 320 K. The free parameter b

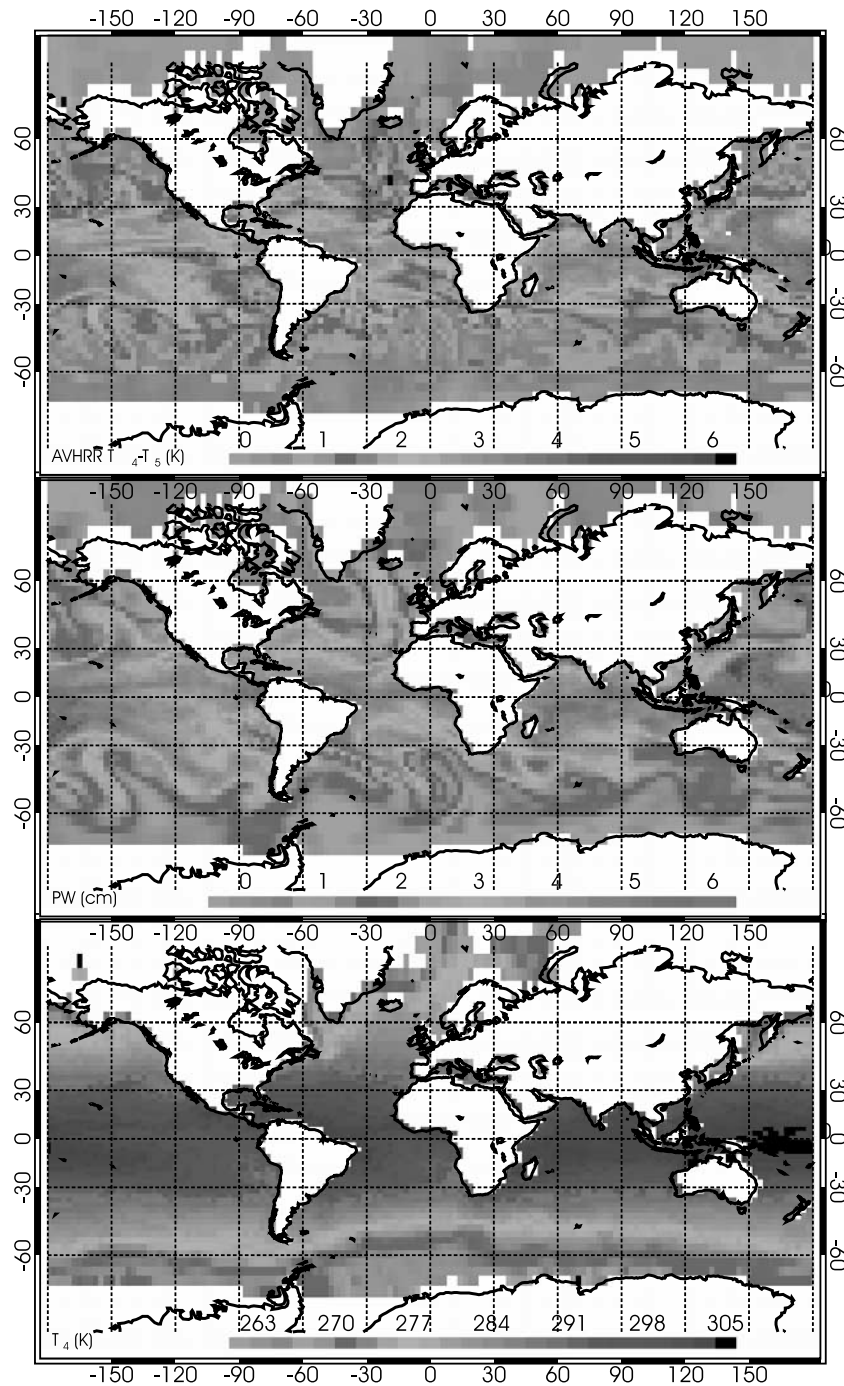


Figure 7. Global distributions of 11–12 μm brightness temperatures (T_4 – T_5 , top panel), precipitable water (cm, middle panel), and 11 μm brightness temperature (K, bottom panel) for 26 December 1996 at 0000 UT. See color version of this figure at back of this issue.

essentially determines the value of the water vapor effect on T_4 – T_5 at the maximum value of T_4 . Hence b can be determined directly from the image data, allowing realistic flexibility on the size of the water vapor correction determined by this semiempirical approach. As shown by *Prata and Grant* [2001b], these relationships can form the basis for an atmospheric correction on any image, where first b is determined then ΔT_{wv} evaluated for each pixel. We did this correction on the Montserrat image shown in Figure 2 and obtained a result nearly identical to Figure 2c. In many

specific cases, especially when clear-sky pixels are not present, this method may be a practical solution for the operator who needs results quickly.

[27] Alternatively, there is another way we can estimate the BT shift in real time using the correlation in Figure 8. Clear-sky brightness temperatures of bands 4 and 5 of AVHRR and GOES may be measured in clear-sky areas adjacent to the volcanic clouds. We investigated the use of these clear-sky brightness temperatures to assess the radiance at the volcanic cloud base. The atmosphere above the volcanic cloud is

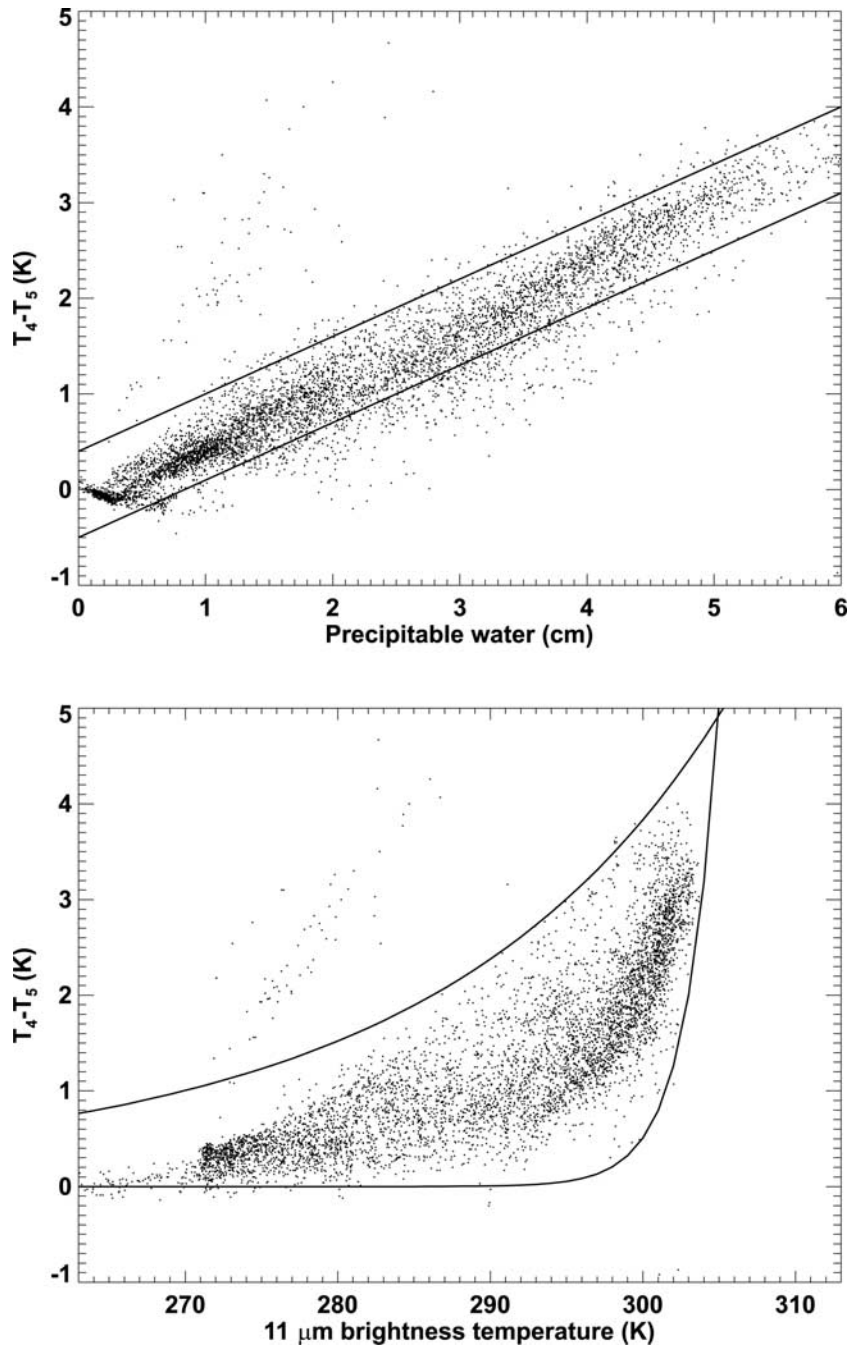


Figure 8. Correlations between precipitable water (in cm) and T_4-T_5 (top panel), and T_4 and T_4-T_5 (bottom panel).

generally thin and very dry and therefore does not influence the radiation transfer much. Although it seems workable in general, a problem with this approach is that there are often climatological clouds near volcanic clouds and background environments vary significantly. Thus clear-sky pixels may be hard to define and locate in some images.

[28] To investigate how water vapor affects the clear-sky band 4 BT and BTDs of AVHRR and GOES, and how real-time scene-based band 4 BT and BTDs can be used in our retrieval model, we found clear-sky pixels in the Montserrat and Spurr volcanic cloud areas based on our image interpretation experience. These clear-sky pixels are located close

to the Montserrat and Spurr volcanic clouds and reflect the environment immediately surrounding the volcanic clouds. Table 2 lists the mean and range of BT 4, BT 5, and BTD of these clear-sky pixels along with the band 4 BT, band 5 BT, and BTD values simulated from MODTRAN.

[29] Table 2 shows that (1) the clear-sky pixels have a very narrow range of band 4 BT in both Montserrat and Spurr volcanic cloud areas. The mean band 4 BT of these clear-sky pixels are 296.2 and 274.4 K, respectively, for Montserrat and Spurr volcanic cloud areas; these two values are slightly larger than the band 4 BT (292.6 and 273.6K) simulated from MODTRAN; and (2) the BTD of clear-sky

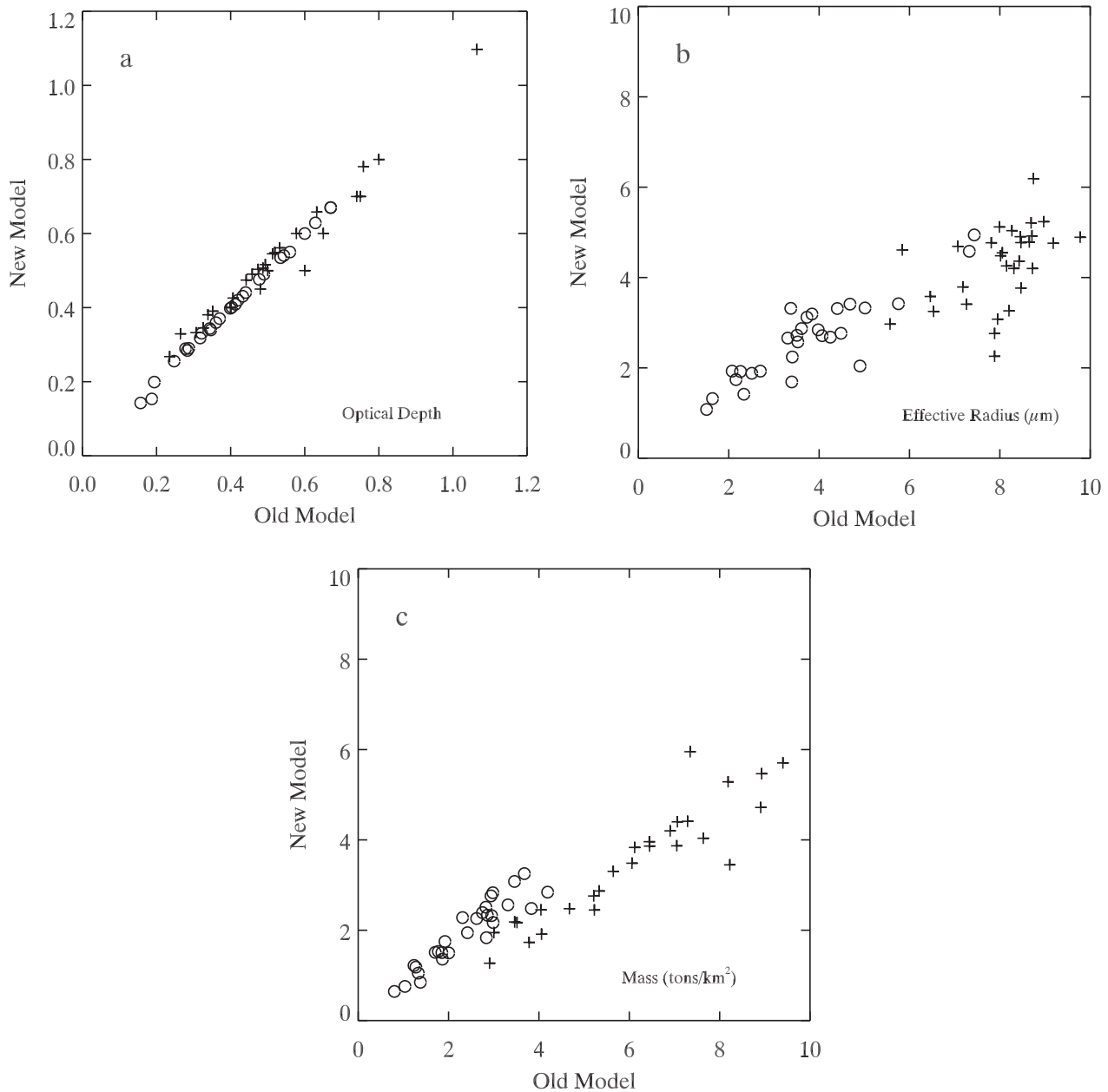


Figure 9. Comparisons of retrieval results of selected representative volcanic cloud pixels detected by the old cutoff procedure and the new one. (a) Optical depth. (b) Effective radius (μm). (c) Mass in tons per square kilometer. The samples from Montserrat volcanic cloud are represented by plus signs; the samples from Spurr volcanic cloud are represented by circles.

pixels varies significantly. For the Montserrat volcanic cloud the BTD is in the range of 0.72–2.85 K, the BTD for the Spurr volcanic cloud is in the range of -0.39 –0.90 K, while BTD simulated by MODTRAN for Montserrat and Spurr volcanic cloud areas is 3.07 and 0.98 K, respectively. These results show that standard average atmospheric profiles approximate the real-time measurements using clear-sky pixels.

[30] The analysis above suggests that minimum and maximum values of these clear-sky pixels may be used for real-time retrievals. The real-time brightness temperatures of bands 4 and 5 are (294.91; 292.06) and (273.23; 272.33) for the Montserrat and Spurr volcanic clouds,

respectively, while MODTRAN-simulated brightness temperatures of bands 4 and 5 at cloud bases are (292.62; 289.57) and (273.63; 272.65) separately for Montserrat and Spurr volcanic clouds. The bands 4 and band 5 brightness temperatures simulated from MODTRAN are very close to the pair of values from clear-sky pixels.

6. Results

6.1. Pixel Comparison of Optical Depths and Effective Radii Retrieved From Old and New Models

[31] To compare retrieval results (optical depth, effective radius, and mass) from the old model and the improved one,

Table 3. Comparison of Retrieval Results From Old and New Model for Selected Pixels

| Volcanic Cloud | Property | Difference, % | | |
|----------------|---------------------------------|---------------|---------|--------|
| | | Minimum | Maximum | Mean |
| Montserrat | optical depth | -16.67; | 24.39 | 3.32 |
| | effective radius, μm | -71.36; | -21.06 | -46.32 |
| | mass in one pixel, ton | -58.07; | -18.79 | -41.84 |
| Spurr | optical depth | -17.99; | 3.91 | -0.70 |
| | effective radius, μm | -58.39; | -1.64 | -28.01 |
| | mass in one pixel, ton | -38.42; | -1.17 | -18.03 |

pixels were selected from Montserrat and Spurr volcanic clouds. All the selected pixels had negative BTD values, so both models could be used.

[32] Earth surface temperature under the volcanic cloud is set at 292 K [Mayberry *et al.*, 2002] in the old model for the Montserrat volcanic cloud. In the new model, the brightness temperatures of the surface for bands 4 and 5 of GOES are 292.62 and 289.57 K, respectively; these two values come from MODTRAN simulations. The cloud top temperature is set at 240 K based on early measurements of the volcanic cloud [Mayberry *et al.*, 2002]. For the Spurr cloud using the old model, Earth surface temperature is 273 K [Schneider *et al.*, 1995], and brightness temperatures of the surface for bands 4 and 5 of AVHRR are 273.63 and 272.65 K, respectively. These values also come from MODTRAN simulations. The cloud top temperature for the Spurr volcanic cloud is set at 200 K; this value comes from the coldest part of the volcanic cloud measured hours earlier.

[33] Figure 9 illustrates the pixel comparisons of optical depth, effective radius, and mass in tons/km² from the old retrieval model and the new one. The optical depths retrieved from these two models are highly correlated and show little difference (Figure 9a). The effective radii from the new model are consistently smaller than those from the old model, especially for the Montserrat volcanic cloud (Figure 9b). The masses retrieved from the new model are systematically smaller than those from the old model (Figure 9c); the decrease in mass in tons/km² mainly results from the smaller effective radius retrieved from the new model.

[34] Table 3 lists the range and mean of differences in optical depth, effective radius, and mass retrieved from these two retrieval models for the selected pixels. It shows that the differences in retrieved results for the Montserrat volcanic cloud are larger than those for the Spurr volcanic cloud (Table 3); this is because for the Montserrat volcanic cloud, the clear-sky BTD is ~ 3.1 K, while the Spurr

volcanic cloud has a clear-sky BTD ~ 1.0 K; as a result, the new model performs a larger atmospheric correction for the Montserrat volcanic cloud than for the Spurr volcanic cloud.

6.2. Tests on Whole Montserrat and Spurr Volcanic Cloud

[35] The mean optical depth and mean effective radius from the new retrieval model decreased slightly for Spurr (12% for optical depth and 18% for effective radius, Table 4) and markedly for Montserrat (46% for optical depth and 52% for effective radius, Table 4). In spite of all these decreases, the total ash mass in both clouds increased, because the cloud area increases were larger and this offset the decreases in optical depth and size. Spurr ash mass increased by 24% and Montserrat increased by 53%. This comparison shows the differential effects of the atmospheric correction in moist and dry atmospheres.

[36] Figure 10 plots the effects of atmospheric correction on all pixels in another format. Figure 10a shows the old retrieval model for the Spurr volcanic cloud, while Figure 10b is the new retrieval model. Corresponding results for Montserrat are in Figures 10c and 10d. Figure 10 shows that (1) the atmospheric corrections affect the retrieval results for the volcanic cloud pixels with higher band 4 BT and BTB ~ 0 much more than those with lower band 4 BT and BTB $\ll 0$. Pixels with higher band 4 BT and BTB > 0 are typically at the edges of volcanic clouds; (2) atmospheric corrections are significantly larger for the Montserrat volcanic cloud than for the Spurr volcanic cloud, because of the moist tropical atmosphere; and (3) the retrieved mean effective radii from the new model are significantly less than those from the old model for both Montserrat and Spurr volcanic clouds, while mean optical depths do not change very much.

6.3. Comparison of Distributions of Optical Depth and Particle Size

[37] Maps of optical depths and effective radii retrieved from old and new retrieval models for Montserrat and Spurr volcanic clouds are shown in Figures 11 and 12. For the Montserrat volcanic cloud the old cutoff procedure only detects the core of the volcanic cloud (Figure 11a) with optical depth > 0.4 ; the additional volcanic cloud area detected by the new cutoff procedure (Figure 11c) mainly has an optical depth < 0.4 (the approximate lower limit for optical depth in this analysis is 0.05). The distribution of effective radius (Figure 11b) from the old retrieval model suggested that some larger particles are located at the edge

Table 4. Retrieval Results for Montserrat and Spurr Volcanic Clouds

| Cutoff and Retrieval Model | Montserrat | | | Spurr | | |
|---|------------|--------|--------|-------|--------|--------|
| | Old | New | New | Old | New | New |
| MODTRAN or BTB method | | MOD. | BTB | | MOD. | BTB |
| Areas ($\times 10^3$ km ²) | 13.2 | 74.6 | 74.6 | 187.9 | 283.7 | 283.7 |
| Cloud top temperature, K | 240 | 240 | 240 | 200 | 200 | 200 |
| BT 4, K | 292 | 292.62 | 294.91 | 272 | 273.63 | 273.23 |
| BT 5, K | 292 | 289.57 | 292.06 | 272 | 272.65 | 272.33 |
| Mean optical depth | 0.392 | 0.264 | 0.321 | 0.378 | 0.332 | 0.320 |
| Mean effective radius, μm | 8.452 | 4.003 | 5.438 | 3.721 | 3.038 | 3.121 |
| Mean mass in one pixel, ton | 86.25 | 23.22 | 36.47 | 2.16 | 1.98 | 1.90 |
| Total mass, KT | 70.9 | 108.3 | 170.0 | 370.9 | 463.0 | 445.9 |

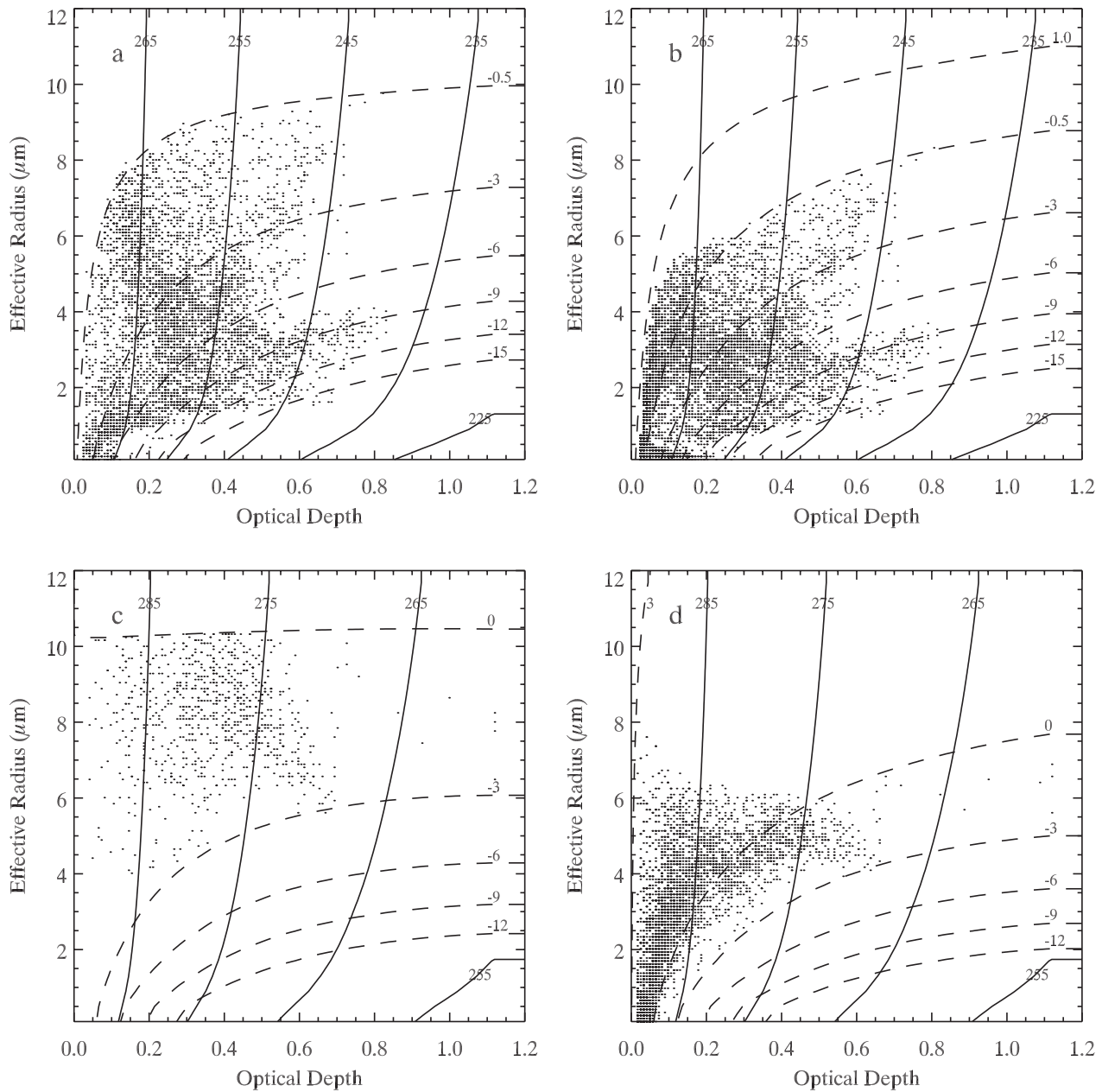


Figure 10. Optical depth versus effective radius plots of volcanic cloud pixels with contours of band 4 brightness temperatures and BTDs. (a) Old retrieval model with Spurr volcanic cloud pixels. (b) New retrieval model with Spurr volcanic cloud pixels. (c) Old retrieval model with Montserrat volcanic cloud pixels. (d) New retrieval model with Montserrat volcanic cloud pixels.

of the volcanic cloud detected by the old cutoff procedure, a result we consider to be unlikely. The distributions of effective radius from the new model (Figure 11d) show that the larger particles are generally at the center of the volcanic cloud.

[38] For the Spurr volcanic cloud the volcanic cloud areas detected by the old cutoff procedure (Figure 12a) and the new cutoff procedure (Figure 12c) show smaller differences. Additional volcanic pixels detected by the new cutoff procedure generally have lower optical depths < 0.3 (Figure 12c). The distribution of effective radii of volcanic area detected by the new cutoff procedure from

the new model (Figure 12d) suggests that even with correction, the thin edges of volcanic clouds can sometimes still contain larger particles. Since these cloud edges have very low optical depths, there is always the possibility that the weak volcanic cloud signal is perturbed by other environmental factors (e.g., sea-salt particles below the volcanic cloud).

7. Discussion

[39] The satellite zenith angle of a pixel depends on the location and latitude of the pixel and its relation to the

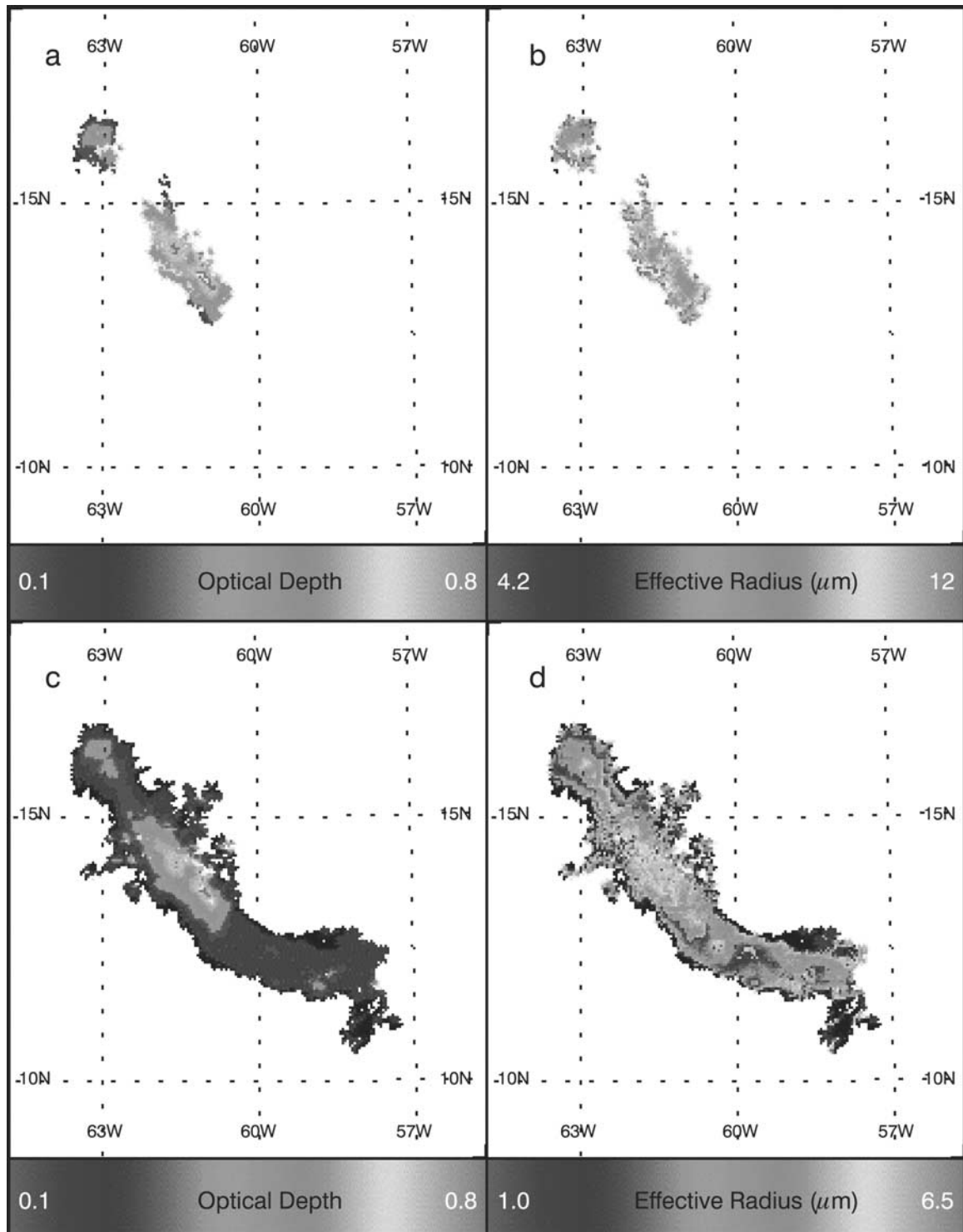


Figure 11. Maps of optical depth and effective radius of Montserrat volcanic cloud. (a) Optical depth, old cutoff, and retrieval model. (b) Effective radius, old cutoff, and retrieval model. (c) Optical depth, new cutoff, and retrieval model. (d) Effective radius, new cutoff, and retrieval model. See color version of this figure at back of this issue.

satellite position. The Spurr volcanic cloud was located at the edge of an AVHRR swath, and the computed satellite zenith angles of the volcanic cloud pixels are in the range of 55° – 65° . The Montserrat volcanic cloud was at the center of the GOES image with the satellite nearly directly over-

head, the volcanic cloud pixels have satellite zenith angles between 20° and 25° .

[40] To evaluate the effect of satellite zenith angle on band 4 BT and BTM and to investigate their influences on volcanic cloud retrievals, we simulated the clear-sky band 4

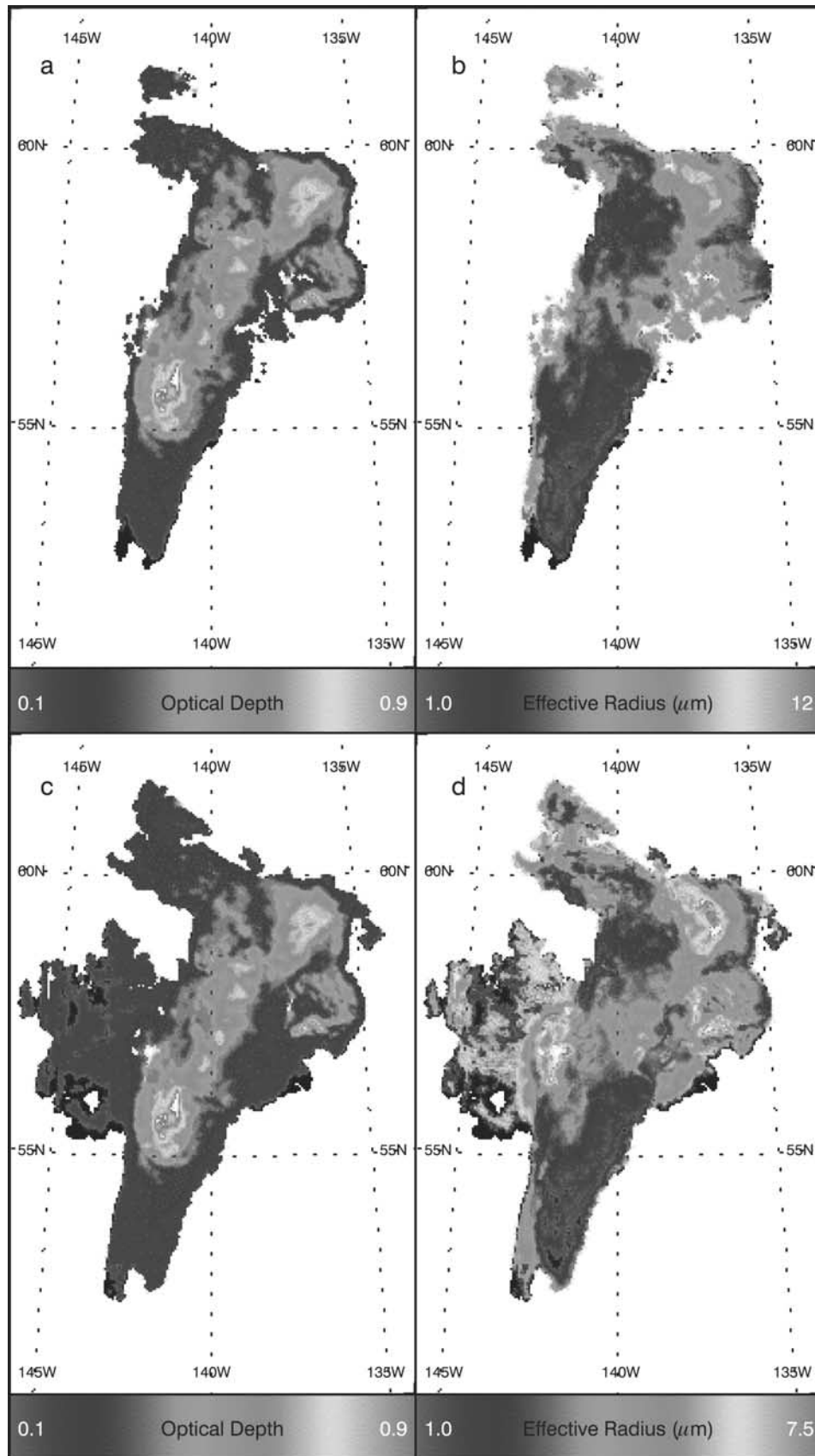


Figure 12. Maps of optical depth and effective radius of Spurr volcanic cloud. (a) Optical depth, old cutoff, and retrieval model. (b) Effective radius, old cutoff, and retrieval model. (c) Optical depth, new cutoff, and retrieval model. (d) Effective radius, new cutoff, and retrieval model. See color version of this figure at back of this issue.

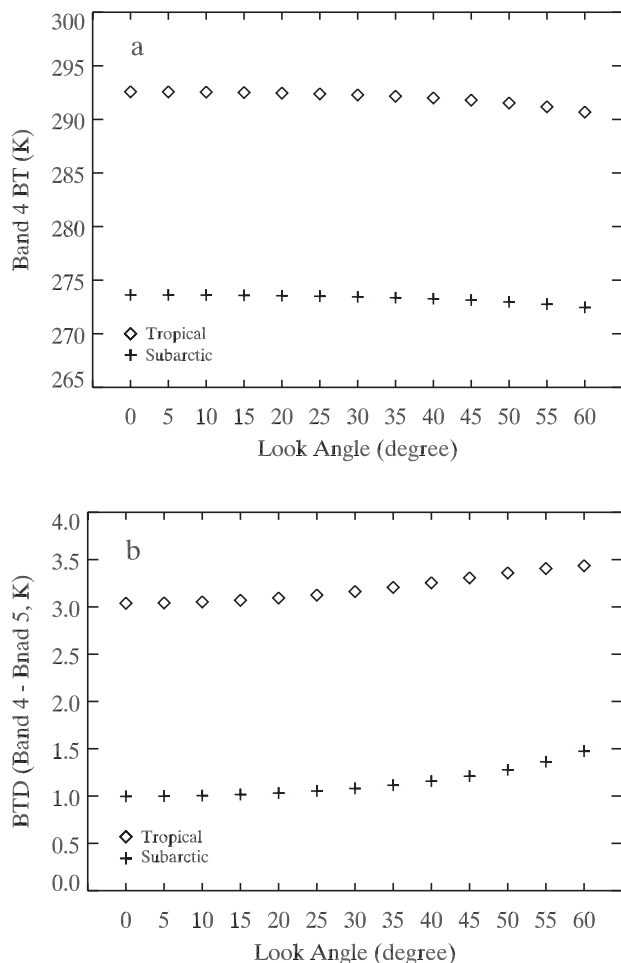


Figure 13. Effects of satellite view angle on band 4 brightness temperatures and BTDs of clear sky. (a) Band 4 brightness temperatures. (b) BTD (band 4 – band 5).

BT and BTD using MODTRAN with different zenith angles for tropical and subarctic environments. Results are shown in Figure 13. Because the Montserrat volcanic cloud pixels have smaller satellite zenith angles and the band 4 wavelengths of AVHRR and GOES are nearly identical, the simulations are only performed for AVHRR wavelengths.

[41] Figure 13a shows that the band 4 BT decreases as the satellite zenith angle increases. The decrements in band 4 BT can reach maxima of ~ 1.9 and ~ 1.2 K, respectively, for tropical and subarctic environments. Figure 13b shows that BTD increases with zenith angle for both tropical and subarctic atmospheres. The maximum increments in BTD are ~ 0.4 and ~ 0.5 K, respectively. Thus our simulations show that for two identical pixels, the one with a larger satellite zenith angle will show a larger BTD and smaller band 4 BT than that of the smaller satellite zenith angle.

[42] Theoretically, a larger BTD will result in a smaller effective radius, and a lower band 4 brightness temperature will result in a smaller optical depth from our retrieval models. The retrieval results of the Montserrat volcanic cloud should not be affected significantly by the satellite zenith angle effects, because the satellite zenith angles are so small that the band 4 BT and the BTD shift are constant for all observed volcanic cloud pixels. For the Spurr

volcanic cloud the optical depths, effective radii, and masses for pixels with larger satellite zenith angles may be slightly overestimated, but even in the case of the maximum 0.5 K difference in BTD and 1.2 K difference in band 4 BT, the introduced errors should be insignificant.

[43] We mentioned above that the measured band 4 BT and BTD of the clear-sky pixels surrounding the volcanic clouds may be used in real-time application of the new retrieval model instead of the MODTRAN simulation. An alternative is to evaluate b from the image data and apply a pixel-by-pixel correction using equations (5) and (6). These two methods are closely equivalent. Using the image data approach has two advantages. It eliminates the need for MODTRAN runs and also it can actually measure water vapor differences in successive data sets. To explore this approach, we compare the retrieved results (optical depths, effective radii, and masses) from the new retrieval model using the measured band 4 BT and BTD of the clear-sky pixels with results from MODTRAN simulations. The bands 4 and 5 BT simulated from the MODTRAN are 292.62 and 289.57 K, respectively, and for the Montserrat volcanic cloud, the real-time bands 4 and 5 BT from clear-sky pixels are 294.91 and 292.06 K. For the Spurr volcanic cloud the MODTRAN-simulated bands 4 and 5 BT are spectrally 273.63 and 272.65 K; the real-time BT 4 and BT 5 from the Spurr volcanic cloud image are 273.23 and 272.33 K. Table 4 lists the retrieval results using the real-time and MODTRAN-simulated values for the whole Montserrat and Spurr volcanic clouds detected by the new cutoff procedure. For the Spurr volcanic cloud the mean optical depth, mean effective radius, and mean pixel mass from the real-time values are very close to those from MODTRAN-simulated values; the differences in retrieved results are all less than 5%. For the Montserrat volcanic cloud the mean optical depth, mean effective radii, and mean pixel mass increase by 22, 39, and 57%, respectively. The larger difference in retrieved results for Montserrat volcanic cloud results from the larger difference between the real-time clear-sky values and the MODTRAN-simulated values. We suggest that the difference could reflect a variable water vapor content, where the conditions at Montserrat differed from the tropical average profile selected in the MODTRAN runs.

[44] The results above suggest that the band 4 BT and BTD of real-time clear-sky pixels can be used in retrievals of volcanic clouds located in high-latitude regions without introducing significant errors. We aim to observe and evaluate the range of possible scenarios by using the real data to improve on model atmospheric profiles. More work needs to be done on how to use the real-time image data to evaluate the radiances at the volcanic cloud base in order to get reliable results.

8. Conclusions

1. A new discrimination procedure for volcanic clouds with atmospheric correction was developed. Without atmospheric corrections, the old discrimination procedure only detects cores of the volcanic clouds, especially in tropics. The cores of the volcanic clouds have negative BTD and have higher optical depths, while additional volcanic cloud edges detected by the atmospherically corrected new cutoff

procedure can have positive BTD and have lower optical depth. For one Montserrat volcanic cloud, an atmospherically corrected cutoff procedure detected a volcanic cloud area several times larger than an uncorrected procedure. For the Spurr eruption the new cutoff procedure detected an area about 50% larger than that from the old cutoff procedure. The new cutoff procedure is important for accurate depiction of volcanic clouds and for aviation safety. The increased volcanic cloud areas detected by the atmospherically corrected cutoff procedure are supported by independent remote sensing studies.

2. A new retrieval model with an atmospheric correction was also developed. Both the new and the old retrieval models used band 4 brightness temperatures and BTDs of AVHRR and GOES. The major difference in the two models is that the new model considers the transmittance differences in both thermal bands of GOES and AVHRR, while the old model assumes that the atmosphere is transparent at the two wavelengths.

3. For both Spurr and Montserrat volcanic clouds the optical depths from the old and new retrieval models are nearly identical, but the effective radii and pixel masses from the new model are less. Differences for Montserrat volcanic cloud are larger than those for the Spurr volcanic cloud. Atmospherically corrected retrievals yield lower values of optical depths and effective radii for the Spurr and Montserrat volcanic clouds. In spite of this, the total ash masses in volcanic clouds for atmospherically corrected conditions increase, because the increased volcanic cloud areas offset the decreases in optical depth and size. The total mass increases for Montserrat and Spurr volcanic clouds are 53% and 24%, respectively. The atmospheric corrections mainly affect volcanic cloud pixels with higher BT 4 and BTD ~ 0 and are most critical for the small volcanic clouds and for those in tropical regions.

4. Clear-sky band 4 BT and BTD are dependent on satellite zenith angle. The band 4 BT decreases as the satellite zenith angle increases, while the BTD increases as the zenith angle increases. The satellite zenith angle of Montserrat volcanic cloud pixels do not significantly affect the retrieval results, because these volcanic cloud pixels have smaller satellite zenith angles ($< 25^\circ$). If the retrievals are applied in the tropics for GOES 8 at high satellite zenith angles, a correction is needed. The band 4 BT and BTD in the dry subarctic regions do not change significantly even at maximum satellite zenith angles.

5. Practical use of the new retrieval model can be done with band 4 BT and BTD from average MODTRAN profiles or from real-time measurement of clear-sky pixels on the images. The retrieval results from real-time band 4 BT and BTD are nearly identical to those from MODTRAN-simulated values for Spurr volcanic cloud. For the Montserrat volcanic cloud the retrieval results from real-time band 4 BT and BTD are larger than those from MODTRAN-simulated values; the average increases in optical depth, effective radius, and pixel mass are about 22, 39, and 57%, respectively. These results represent only one day's atmospheric corrections, so a much more comprehensive evaluation must be done to show conclusively that real-time measurements of band 4 BT and BTD adequately reflect the variations of water vapor in lower troposphere. We have done simulations to show that BTD and

precipitable water values on particular days are strongly correlated.

9. Future Work

[45] We plan to develop methods for implementing atmospheric corrections into automatic or semiautomatic conversions to allow real-time use of this algorithm for ash cloud hazard mitigations. We believe they will be more accurate and will more faithfully outline the 2-D boundaries of volcanic clouds.

[46] **Acknowledgments.** NASA and NSF (EAR97-25682) supported this research. Vince Realmuto encouraged us to develop this scheme. Gregg Bluth, Bruce Rafert, Matt Watson, and two anonymous reviewers helped improve the text.

References

- Ackerman, S. A., and K. I. Strabala, Satellite remote sensing of H₂SO₄ aerosol using the 8- to 12- μ m window region: Application to Mount Pinatubo, *J. Geophys. Res.*, **99**, 18,639–18,649, 1994.
- Baran, A. J., J. S. Foot, and P. C. Dibben, Satellite detection of volcanic sulfuric acid aerosol, *Geophys. Res. Lett.*, **20**, 1799–1801, 1993.
- Baxter, P. J., et al., Cristobolite in volcanic ash of Soufrière Hills volcano, Montserrat, British West Indies, *Science*, **283**, 1142–1145, 1999.
- Berk, A., L. S. Bernstein, and D. C. Robertson, MODTRAN: A moderate resolution model for LOWTRAN 7, *AFGL Tech. Rep.*, AFGL-TR-89-0122, U. S. Air Force Geophys. Lab., Hanscom Air Force Base, Mass., 1989.
- Bonadonna, C., et al., Tephra Fall in the 1995–1998 eruption of the Soufrière Hills volcano, Montserrat, in *The Eruption of the Soufrière Hills Volcano, Montserrat, 1995-99*, edited by T. Druitt and P. Kokelaar, *Mem. Geol. Soc., London*, in press, 2002.
- Cole, P. D., et al., Pyroclastic flows generated by gravitational instability of the 1996–1997 lava dome of Soufrière Hills volcano, Montserrat, *Geophys. Res. Lett.*, **25**(18), 3425–3428, 1998.
- Coll, C., and V. Casselles, A split-window algorithm for land surface temperature from advanced very high resolution radiometer data: Validation and algorithm comparison, *J. Geophys. Res.*, **102**, 16,697–16,713, 1997.
- Jensen, J. R., *Introductory Digital Image Processing: A Remote Sensing Perspective*, Prentice-Hall, Old Tappan, N. J., 1996.
- Kidder, S. Q., and T. H. Vonder Haar, *Satellite Meteorology: An introduction*, Academic, San Diego, Calif., 1995.
- Krotkov, N. A., O. Torres, C. Sefstor, A. J. Krueger, A. Kostinski, W. I. Rose, G. J. Bluth, D. Schneider, and S. J. Schaefer, Comparison of TOMS and AVHRR volcanic ash retrievals from the August 1992 eruption of Mt. Spurr, *Geophys. Res. Lett.*, **26**(4), 455–458, 1999.
- Liou, K. N., *An Introduction to Atmospheric Radiation*, Academic, San Diego, Calif., 1980.
- Mayberry, G. C., W. I. Rose, and G. J. S. Bluth, Dynamics of the volcanic and meteorological clouds produced by the December 26, 1997 eruption of Soufrière Hills volcano, Montserrat, W. I., in *The Eruption of the Soufrière Hills Volcano, Montserrat, 1995–99*, edited by T. Druitt and P. Kokelaar, *Mem. Geol. Soc., London*, **21**, 539–555, 2002.
- McMillan, L. M., and C. Dean, Evolution of a new operational technique for producing clear radiances, *J. Appl. Meteorol.*, **20**, 1005–1014, 1982.
- Neal, C. A., R. G. McGimsey, C. A. Gardner, M. L. Harbin, and C. J. Nye, Tephra-fall from 1992 eruptions of Crater Peak, Mount Spurr Volcano, AK: A Preliminary report on distribution, stratigraphy and composition, *U. S. Geol. Surv. Bull.*, **2139**, 1994.
- Parol, F., J. C. Buriez, and Y. Fouquart, Information content of AVHRR channels 4 and 5 with respect to the effective radius of cirrus cloud particles, *J. Appl. Meteorol.*, **30**, 973–984, 1991.
- Pollack, J. B., O. B. Toon, and B. N. Khare, Optical properties of some terrestrial rocks and glasses, *Icarus*, **19**, 372–389, 1973.
- Prata, A. J., Observations of volcanic ash clouds using AVHRR-2 radiances, *Int. J. Remote Sens.*, **10**(4–5), 751–761, 1989a.
- Prata, A. J., Radiative transfer calculations for volcanic ash clouds, *Geophys. Res. Lett.*, **16**(11), 1293–1296, 1989b.
- Prata, A. J., and I. F. Grant, Determination of mass loadings and plume heights of volcanic ash clouds from satellite data, *CSIRO Atmos. Res. Tech. Pap.* **48**, 39 pp., Commonw. Sci. and Ind. Res. Organ., Melbourne, Victoria, Australia, 2001a.
- Prata, A. J., and I. F. Grant, Retrieval of microphysical and morphological

- properties of volcanic ash plumes from satellite data: Application to Mt. Ruapehu, New Zealand, *Q. J. R. Meteorol.*, 127, 2001b.
- Rose, W. I., A. J. Prata, G. J. S. Bluth, L. R. Coke, and D. J. Schneider, Atmospheric corrections for two band infrared volcanic cloud discriminations and retrievals, *Eos Trans. AGU*, 78(46), F818, Fall Meet. Suppl., 1997.
- Rose, W., and G. C. Mayberry, Use of GOES thermal infrared imagery for eruption scale measurements, Soufriere Hills, Montserrat, *Geophys. Res. Lett.*, 27(19), 3097–3100, 2000.
- Rose, W. I., A. B. Kostinski, and L. Kelley, Real time C band radar observations of 1992 eruption clouds from Crater Peak, Mount Spurr Volcano, Alaska, *U.S. Geol. Surv. Bull.*, 2139, 19–28, 1995.
- Schneider, D. J., W. I. Rose, and L. Kelley, Tracking of 1992 eruption clouds from Crater Peak vent of Mount Spurr volcano, Alaska, using AVHRR, in *The 1992 Eruptions of Crater Peak Vent, Mount Spurr Volcano, Alaska*, edited by T. E. C. Keith, *U.S. Geol. Surv. Bull.* 2139, 220 pp., 1995.
- Schneider, D. J., W. I. Rose, L. R. Coke, G. J. S. Bluth, I. Sprod, and A. J. Krueger, Early evolution of a stratospheric volcanic eruption cloud as observed with TOMS and AVHRR, *J. Geophys. Res.*, 104, 4037–4050, 1999.
- Seftor, C. J., N. C. Hsu, J. R. Herman, P. K. Bhartia, O. Torres, W. I. Rose, D. J. Schneider, and N. Krotkov, Detection of volcanic ash clouds from Nimbus-7/TOMS reflectivity data, *J. Geophys. Res.*, 102, 16,749–16,760, 1997.
- Sparks, R. S. J., et al., Generation of a debris avalanche and violent pyroclastic density current, in *The Boxing Day Eruption of 26 December 1997 at the Soufrière Hills Volcano, Montserrat*, edited by T. Druitt, R. Soc., London, UK, 2001.
- Wen, S., and W. I. Rose, Retrieval of sizes and total masses of particles in volcanic clouds using AVHRR bands 4 and 5, *J. Geophys. Res.*, 99, 5431–5521, 1994.
- Yamanouchi, T., K. Suzuki, and S. Kawaguchi, Detection of clouds in Antarctica from infrared multispectral data of AVHRR, *J. Meteorol. Soc. Jpn.*, 65, 949–961, 1987.
-
- A. J. Prata, CSIRO, Division of Atmospheric Research, Aspendale, Victoria, Australia.
- W. I. Rose and T. Yu, Department of Geological Engineering and Sciences, 1400 Townsend Drive, Michigan Technological University, Houghton, MI 49931-1295, USA. (raman@mtu.edu)

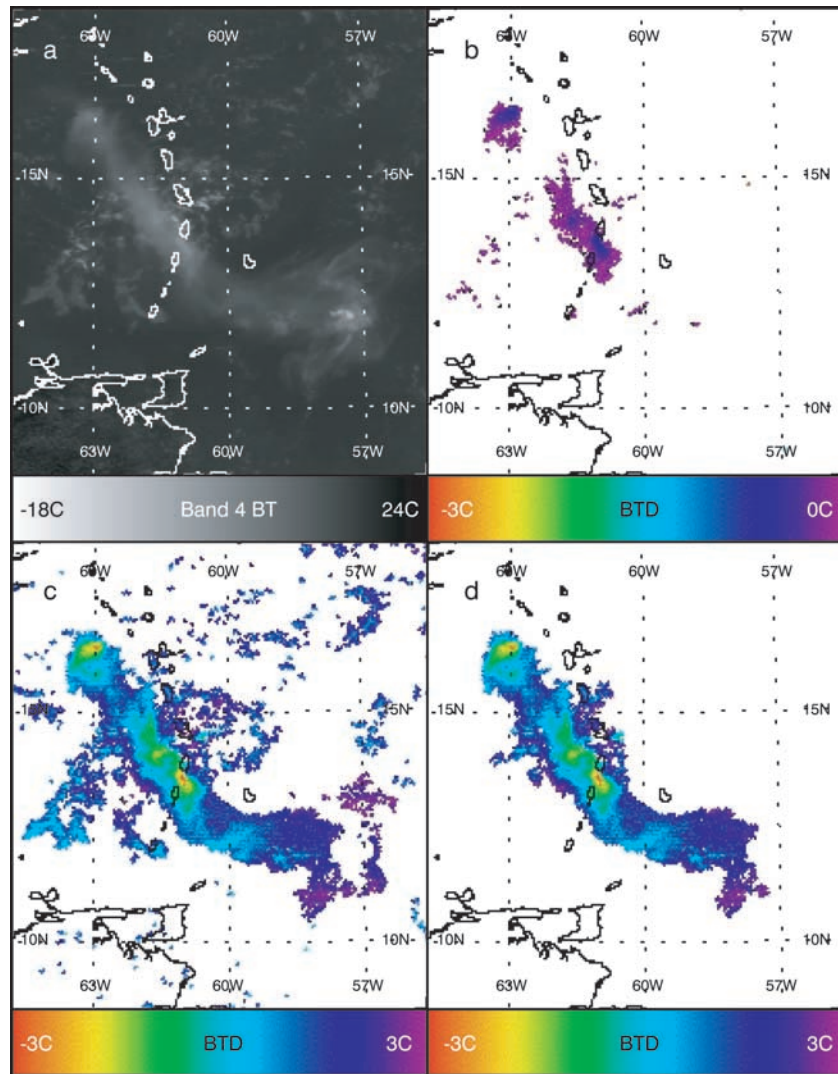
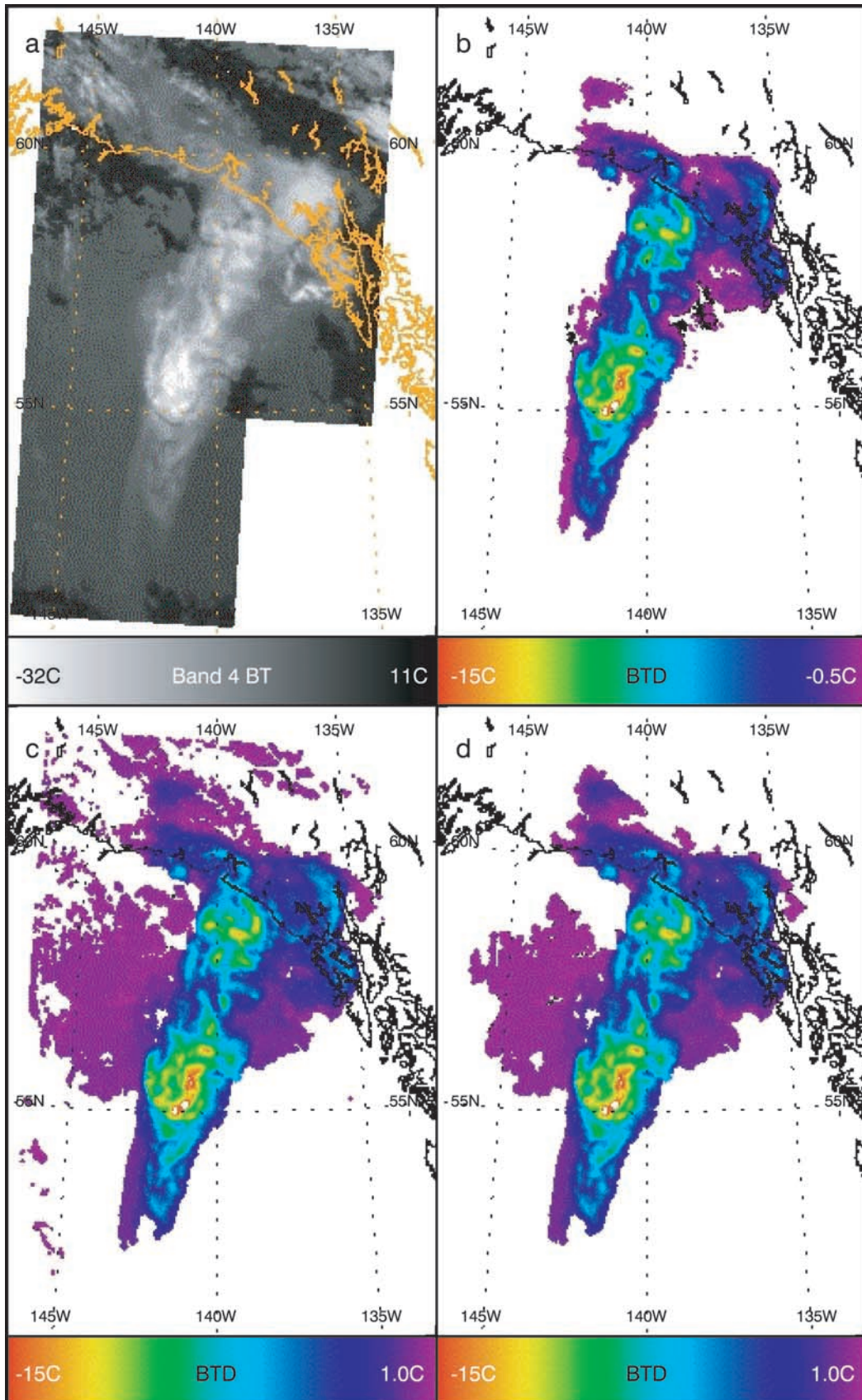


Figure 2. Comparison of new and old cutoff procedures for the Montserrat volcanic eruption. (a) Band 4 image of volcanic cloud area, where the volcanic cloud is depicted as grey over a black ocean background. (b) Volcanic cloud area using the old cutoff procedure. (c) Potential volcanic cloud area using the new cutoff procedure. (d) Final volcanic cloud area from the new cutoff procedure, with image processing to remove false signals (see text for explanation).



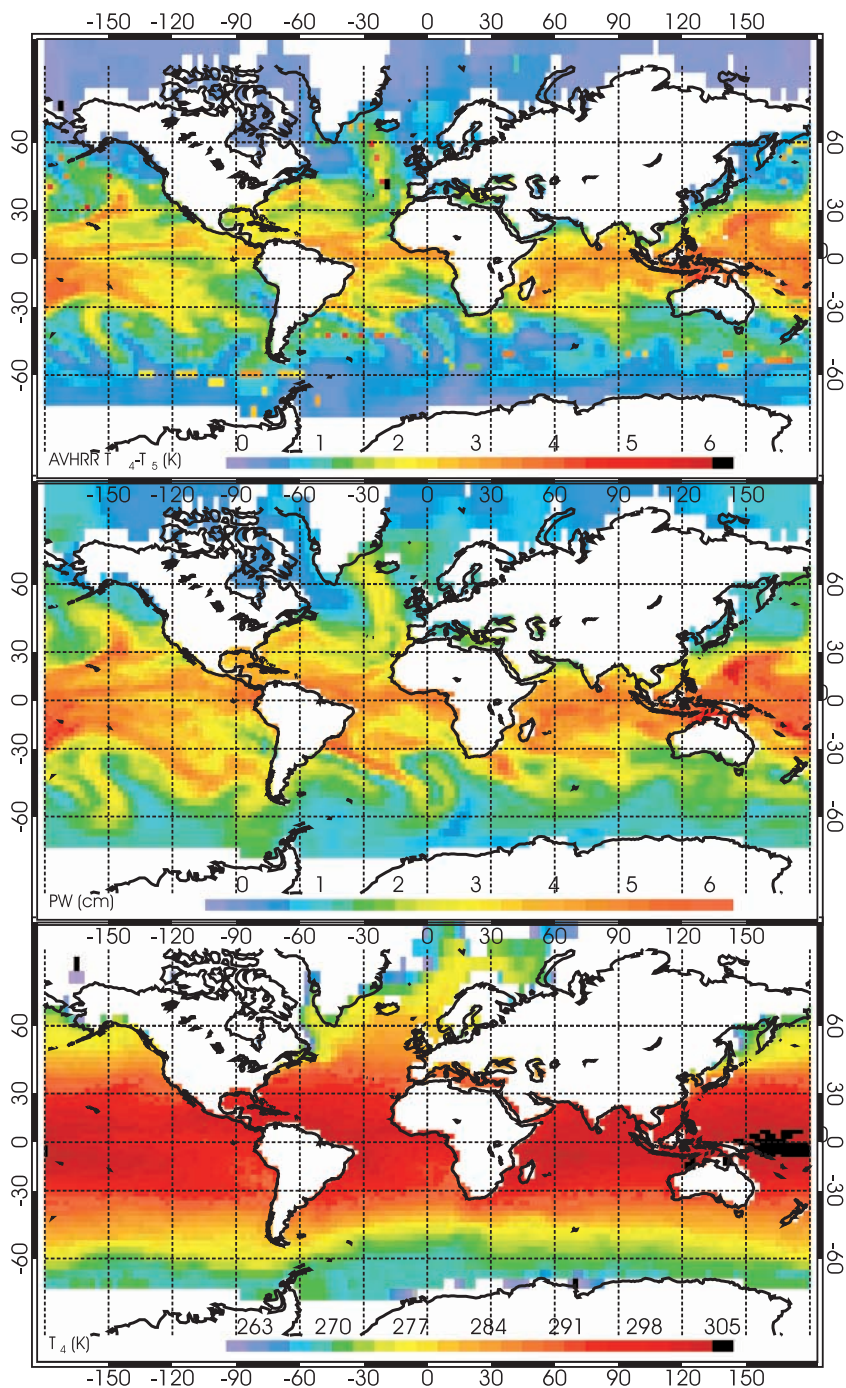


Figure 7. Global distributions of 11–12 μm brightness temperatures ($T_4 - T_5$, top panel), precipitable water (cm, middle panel), and 11 μm brightness temperature (K, bottom panel) for 26 December 1996 at 0000 UT.

Figure 3. (opposite) Results of new and old cutoff procedures for Spurr volcanic eruption. (a) Band 4 image of volcanic cloud. (b) Volcanic cloud area depicted from the old cutoff procedure. (c) Volcanic cloud from the new cutoff procedure. (d) Final volcanic cloud area using the new cutoff procedure, and image processing to remove false signals (see text for explanation).

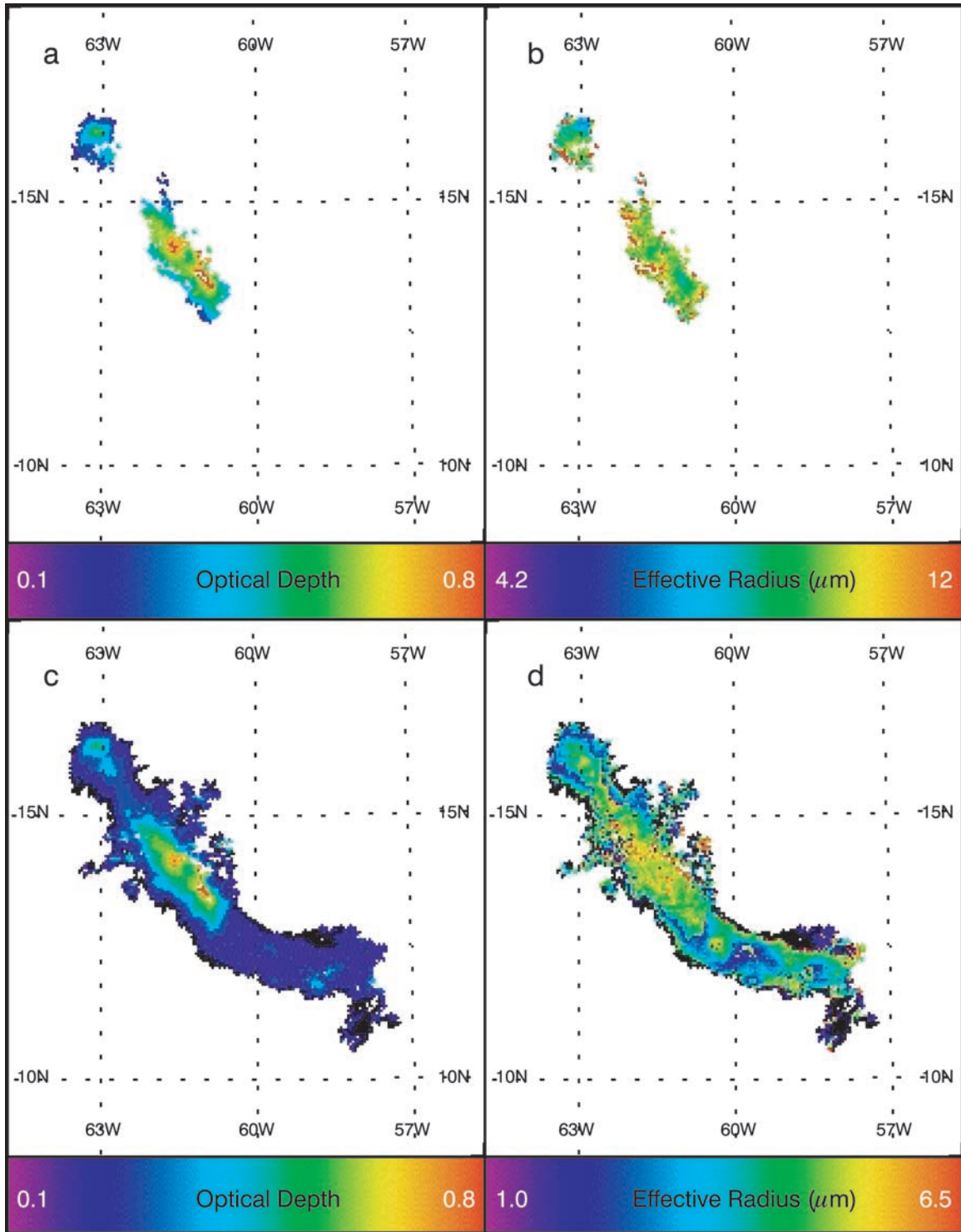


Figure 11. Maps of optical depth and effective radius of Montserrat volcanic cloud. (a) Optical depth, old cutoff, and retrieval model. (b) Effective radius, old cutoff, and retrieval model. (c) Optical depth, new cutoff, and retrieval model. (d) Effective radius, new cutoff, and retrieval model.

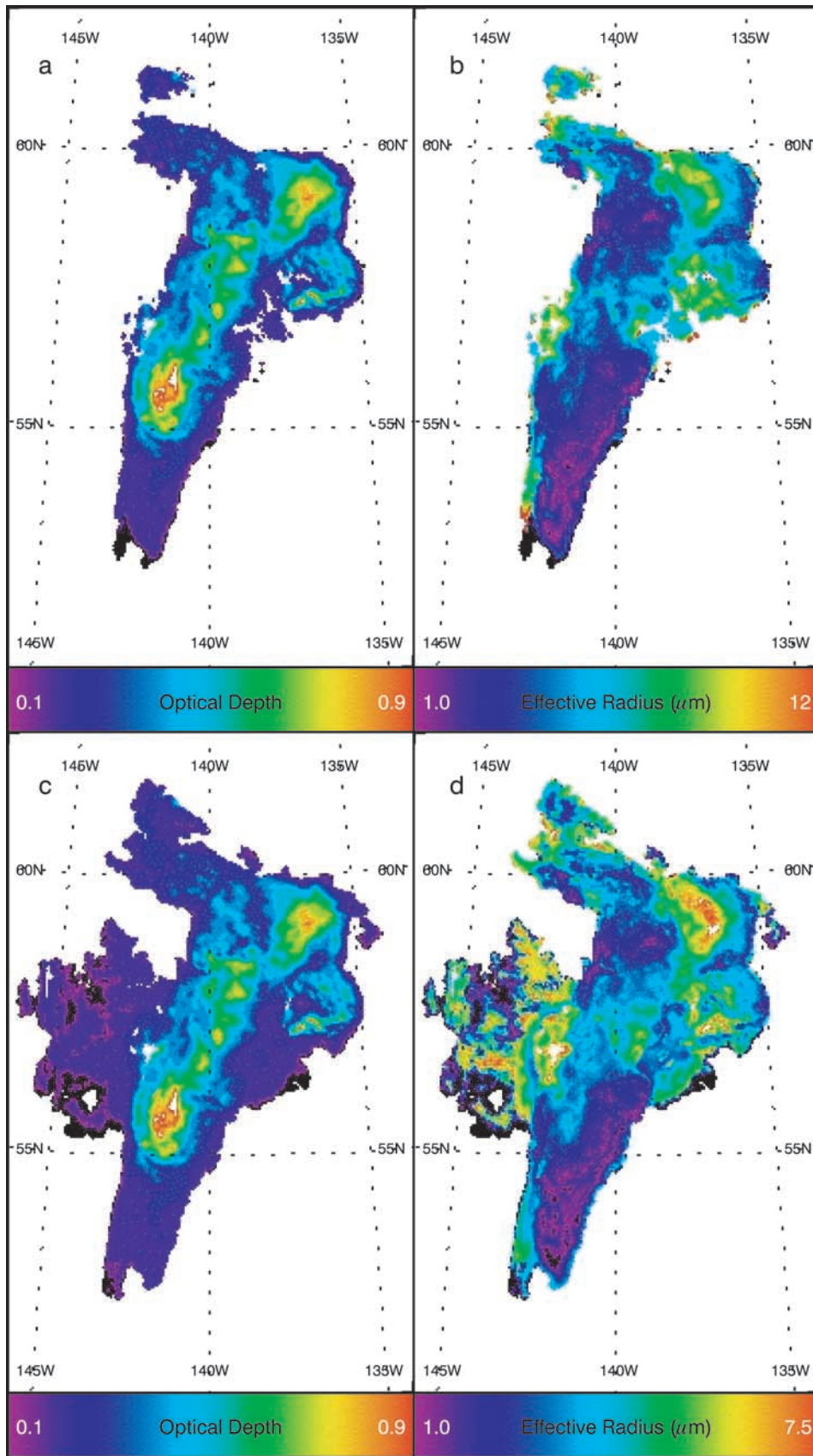


Figure 12. Maps of optical depth and effective radius of Spurr volcanic cloud. (a) Optical depth, old cutoff, and retrieval model. (b) Effective radius, old cutoff, and retrieval model. (c) Optical depth, new cutoff, and retrieval model. (d) Effective radius, new cutoff, and retrieval model.